TM 63-5-4

American Ceramic Society
65th Annual Meeting
Pittsburgh, Pa.,
April 28-May 2, 1963

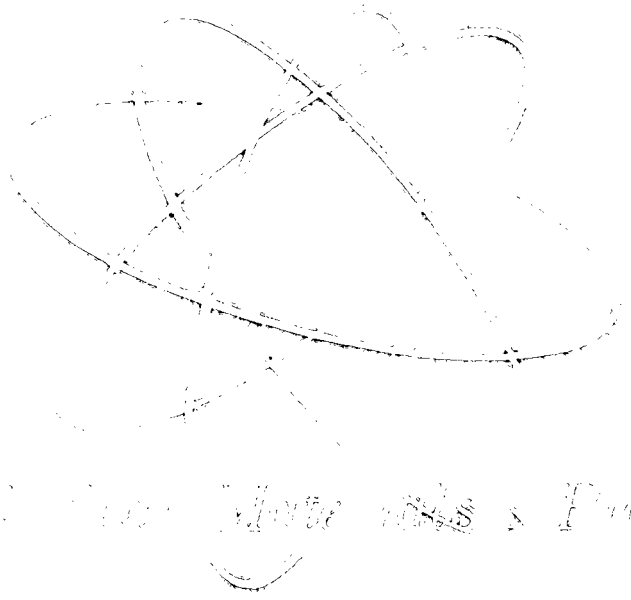

PHYSICAL PROPERTIES OF SINTERED BeO AS INFLUENCED BY MICROSTRUCTURE

by

B. A. Chandler, R. E. Fryxell

For presentation at

Meeting of the American Ceramic Society

April 29, 1963

ADVANCED TECHNOLOGY SERVICES

GENERAL ELECTRIC

DISCLAIMER

PHYSICAL PROPERTIES OF SINTERED BeO AS INFLUENCED BY MICROSTRUCTURE

by R. E. Fryxell and B. A. Chandler

Nuclear Materials and Propulsion Operation,
General Electric Company, Cincinnati, Ohio

* *

Physical properties are presented for extruded and sintered BeO from 25 to 1400°C as a function of porosity (0-15%), grain size (5-100 microns), and grain orientation (random to 80% preferred). The elastic constants and linear thermal expansion are sensitive to the degree of preferred grain orientation. Measurements on polycrystalline specimens have permitted calculation of the anisotropy in single crystals of BeO. Modulus of rupture data are treated in terms of the Knudsen equation, and compressive creep data in terms of the Nabarro-Herring equation, the latter leading to estimates of the diffusion coefficient for Be at 1200°C.

Presented at two meetings of The American Ceramic Society: 15th Pacific Coast Regional Meeting, Seattle, Washington, October 19, 1962, and the 65th Annual Meeting, Pittsburgh, Pennsylvania, April 30, 1963.

The writers are principal engineers, Nuclear Materials and Propulsion Operation, General Electric Company.

I. INTRODUCTION

In connection with a program for evaluating the effects of neutron irradiation on sintered BeO, it was necessary to characterize as accurately as possible the as-fabricated material. For this study, specimens were prepared from two types of powder; (1) type UOX, calcined from $BeSO_4$, and (2) type AOX, calcined from $Be(OH)_2$ which was in turn prepared from the nitrate. These were originally selected as representative commercial raw materials of different degrees of purity, AOX having higher levels of impurities than UOX. In addition, it was learned that UOX powder contains an appreciable amount of needle-like particles (crystallographic c-axis in the direction of the long dimension of the needles) which tend to become aligned in the direction of extrusion if this method of fabrication is used. The growth of these needles in sintering results in a high degree of preferred grain orientation[1]. On the other hand, AOX powder consists of agglomerates which do not result in an oriented structure.

Specimens were in the form of solid cylinders, 3.5 inches long and 0.238 inch diameter after centerless grinding. Some were made by isostatic pressing but most were made by an extrusion process. Details have been reported by Chandler, Duderstadt, and White[2]. Rods fabricated from UOX powder contained 0.5 weight percent MgO which was added as a sintering aid. This addition did not significantly affect the development of preferred grain orientation which has been observed also for undoped UOX after extrusion and sintering[1].

Specimens fabricated from UOX with the MgO addition will be referred to as UOX-MgO. Property data will emphasize UOX-MgO and undoped AOX, but in some instances, reference will be made to other compositions. Properties will be discussed in terms of grain sizes in the range 5-100 microns, and of porosity in the range 0-15 percent.

This report will embrace thermal expansion, elastic constants, strength, and compressive creep, and where applicable differences between the two types of material will be interpreted in terms of preferred grain orientation.

II. THERMAL EXPANSION

(1) Method of Measurement

Linear thermal expansion to 1200°C was measured by a dilatometer technique with specimens of either two inch or 3.5 inch length. The support members were one-eighth inch sapphire rods and the differential sensing element was a strain gage whose displacement was amplified 2000 times on an X-Y recorder chart which provided continuous readings of differential expansion and temperature. Heating and cooling rates were programmed as follows:

75°C per hour up to 400°C
100°C per hour up to 540°C
150°C per hour up to 650°C
200°C per hour above 650°C

Under these conditions, the heating and cooling curves were generally in excellent agreement, rarely differing by more than 0.0002 inch. The return to zero was even better, rarely disagreeing by more than 0.00005 inch from the

starting point. Readings from the chart were converted to net expansion of the BeO using sapphire data given by Creamer[3]. At the time this work was started, the more recent data of Wachtman, Scuderi, and Cleek were not available[4]; these would result in small positive corrections in the low temperature region and small negative corrections at 1200°C. The corrections have not been made, however, inasmuch as they are entirely negligible with respect to the anisotropy calculations presented below.

(2) Experimental Results

The data for twenty-five specimens of extruded AOX were submitted to a multiple regression analysis and yielded the following equation:

$$\% \text{ expansion } (25 \text{ to } T^{\circ}C) = 5.8660 \times 10^{-4} (T-25) + 3.8697 \times 10^{-7} (T-25)^2 - 7.0345 \times 10^{-11} (T-25)^3 \quad (1)$$

A similar treatment was made of the data for eight specimens of isostatic pressed and sintered BeO made from various types of raw material. The following equation resulted:

$$\% \text{ expansion } (25 \text{ to } T^{\circ}C) = 5.9148 \times 10^{-4} (T-25) + 3.5394 \times 10^{-7} (T-25)^2 - 5.1600 \times 10^{-11} (T-25)^3 \quad (2)$$

Typical values calculated from these equations are given in Table I together with 95% confidence limits. Mean thermal expansion coefficients deduced from these data are given in Table II. Also shown in Table I are individual data for twenty-three specimens of UOX-MgO. These have not been submitted to a multiple regression analysis since the phenomenon of preferred grain orientation exposes thermal expansion anisotropy which varies with grain size.

TABLE I

LINEAR THERMAL EXPANSION OF AS-SINTERED BeO

Density, g/cm³	Grain Size, microns	Thermal Expansion from 25 to T°C, percent			
		600°C	800°C	1000°C	1200°C
Extruded					
AOX[a]	2 to 112	0.4519	0.6543	0.8746	1.1094
95% confidence limits		0.0007	0.0007	0.0007	0.0013
UOX-MgO					
2.75	63	0.437	0.629	0.841	1.073
2.94	13	0.436	0.630	0.839	1.069
2.90	11	0.442	0.636	0.847	1.083
2.90	19	0.443	0.634	0.843	1.069
2.56	7	0.438	0.635	0.848	1.085
2.85	38	0.428	0.615	0.823	1.053
2.94	89	0.432	0.616	0.823	1.053
2.91	47	0.427	0.612	0.819	1.046
2.77	5	0.445	0.639	0.851	1.087
2.96	9	0.446	0.643	0.859	1.097
2.72	38	0.432	0.624	0.835	1.063
2.75	63	0.423	0.614	0.824	1.053
2.78	11	0.448	0.642	0.857	1.093
2.93	72	0.422	0.609	0.819	1.048
2.90	49	0.423	0.606	0.810	1.036
2.90	47	0.426	0.611	0.813	1.042
2.97	90	0.428	0.612	0.816	1.038
2.93	76	0.426	0.611	0.818	1.042
2.93	112	0.426	0.612	0.818	1.041
2.91	17	0.440	0.635	0.849	1.081
2.97	90	0.429	0.615	0.821	1.046
2.72	38	0.428	0.626	0.839	1.066
2.94	89	0.420	0.608	0.818	1.041
Isostatic Pressed[b]					
	11 to 34	0.4473	0.6470	0.8695	1.1000
95% confidence limits		0.0025	0.0025	0.0025	0.0045

[a] Average of twenty-five specimens with densities ranging from 2.56 to 2.97 g/cm³.

[b] Average of eight specimens with densities ranging from 2.83 to 2.96 g/cm³.

TABLE II

MEAN THERMAL EXPANSION COEFFICIENTS FOR BeO OF RANDOM GRAIN ORIENTATION

T °C	Mean expansion coefficient from 25 to T°C, 10^{-6} in/in°C	
	extruded	isostatic pressed
600	7.858 ± 0.013*	7.779 ± 0.045*
800	8.443 ± 0.009	8.348 ± 0.032
1000	8.970 ± 0.007	8.875 ± 0.026
1200	9.442 ± 0.011	9.361 ± 0.037

*95% confidence limits.

(3) Discussion of Results

As discussed by Sjodahl and Bartram[1], extruded AOX consists of grains which are essentially randomly oriented irrespective of grain size. Similarly, isostatic pressed BeO including that fabricated from the UOX grade also consists of randomly oriented grains. For both types of specimen, the expansion characteristics did not show a variability with grain size, in accord with the above. This is shown quite convincingly in the exceedingly narrow 95% confidence limits for AOX. Mean thermal expansion coefficients for AOX deduced from equation (1) are shown in Figure 1 together with selected literature data. The present data are in good agreement with those obtained by others, and in fact the latter almost without exception fall within the 95% confidence limits for the individual data points of the present work*.

In contrast to AOX, the UOX-MgO exhibits thermal expansion characteristics which vary with grain size. This is shown in Figure 2 in which the mean thermal expansion coefficient from 25° to 1200°C is plotted versus grain size for both grades of BeO. Since the degree of preferred grain orientation in UOX-MgO varies with grain size, it is clear that these data are reflecting the anisotropic nature of BeO. It thus is possible to deduce the single crystal thermal expansion anisotropy. Boas[11] has shown that the c-axis of an individual crystal contributes to thermal expansion in a given direction in a polycrystalline sample in a manner proportional to $\cos^2\phi$, where ϕ is the angle between the c-axis and the given direction of interest. This is of the

*The 95% confidence limits for individual data points are about twelve times the values quoted which are estimated for the equations.

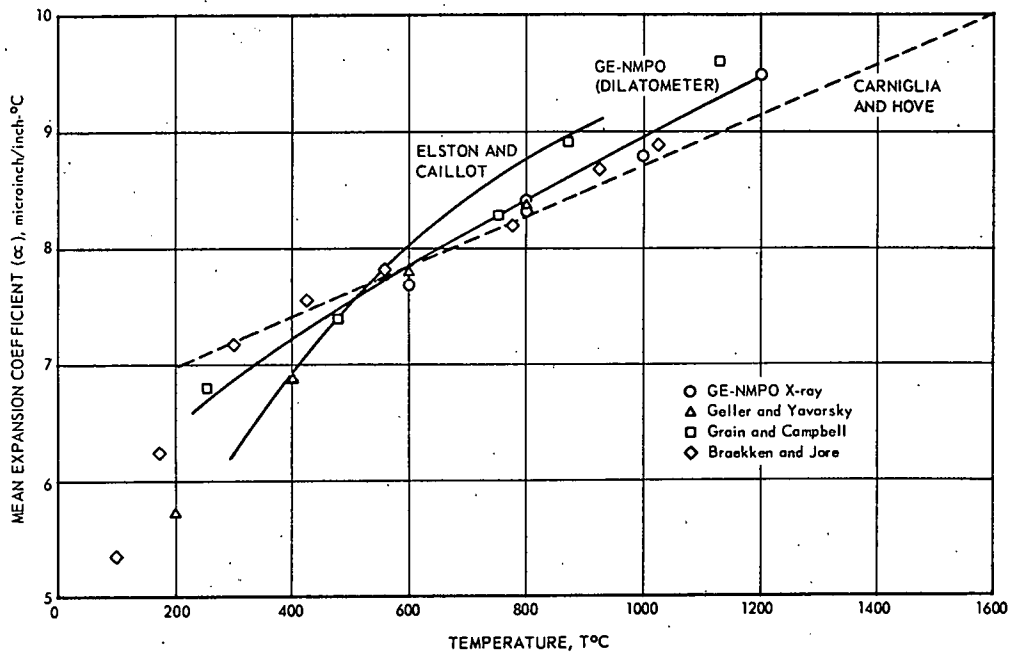

Fig 1.
(Captions attend)

11

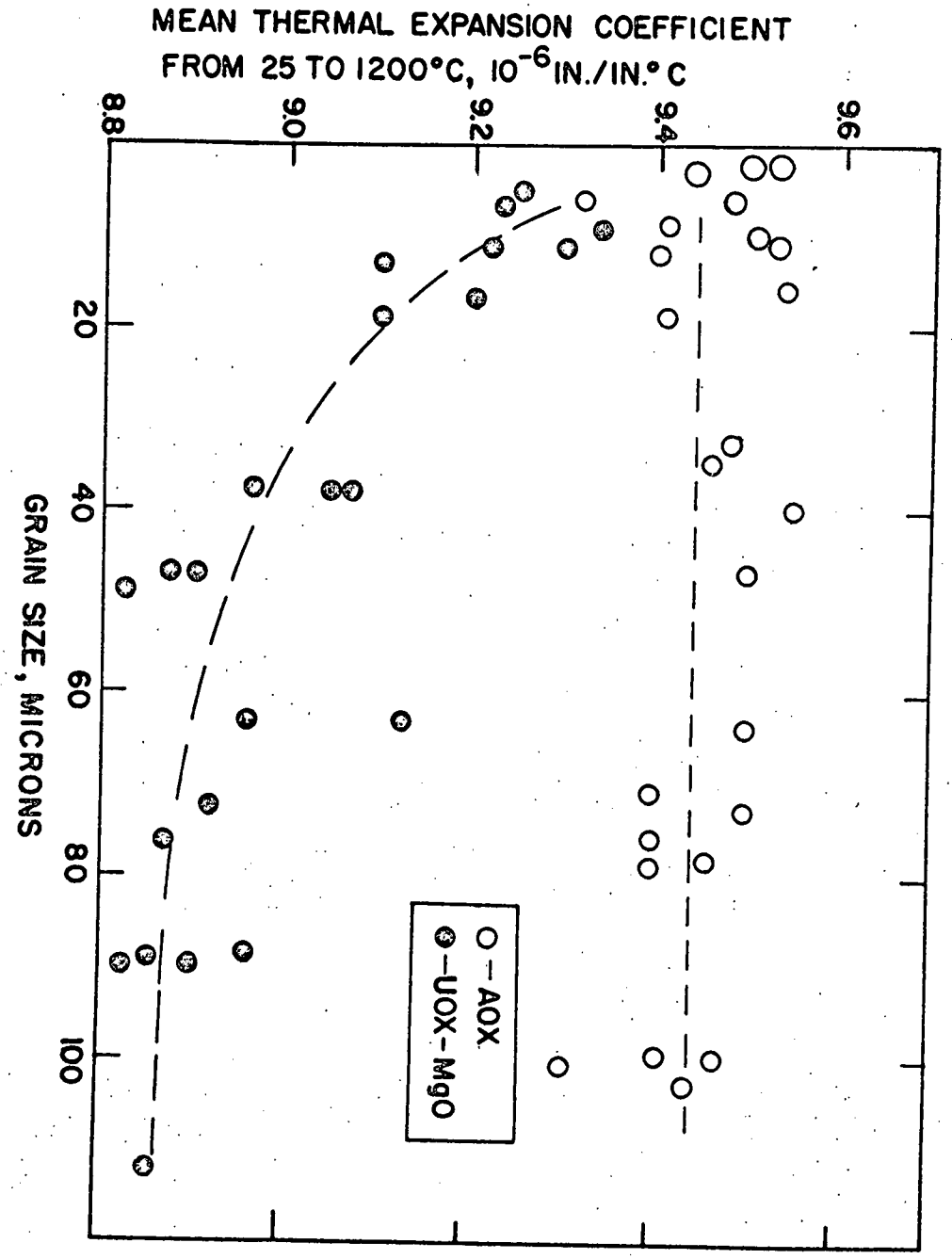
MEAN THERMAL EXPANSION COEFFICIENT
FROM 25 TO 1200°C, 10^{-6} IN./IN.° C
8.8
9.0
9.2
9.4
9.6
GRAIN SIZE, MICRONS
20
40
60
80
100
O — AOX
● — UOX-MgO

Fig. 2

same form as the summation used for calculating percent orientation[1]. The consistency of the data is shown in Figure 3 which indicates the linear relationship between percent orientation and observed linear expansion of polycrystalline samples. Both properties are defined with reference to the longitudinal axis of the specimen. With this summation procedure, differences in the linear expansion between the test specimen and that of a randomly oriented specimen* were combined with the measured percent orientation to obtain an estimate of the c-axis expansion of a single crystal. This value, in turn, led to determining the a-axis expansion. The results for seven specimens are given in Table III in detail and are summarized in Table IV together with data obtained in this laboratory by high temperature X-ray diffractometry[5]. The agreement between the two methods is generally good, at least at 600°C and above, and indicates an anisotropy of about 13% essentially independent of temperature in the range 600 to 1200°C. The results are illustrated in Figures 4 and 5 together with data from the literature. The results presented by Miller[12] were re-evaluated and found to demonstrate anisotropy although this was not recognized in his report.

*The average value for AOX was used as the best available figure. The alternative would be to fit a curve to the seven points shown in Figure 3 without assuming a value for a randomly oriented specimen. This was attempted, and in terms of the anisotropy ratio as defined in Table III, the average difference between the two methods of calculation was only 0.005 in the temperature range of 600 to 1200°C. This is well within the general scatter of the data and is further evidence that AOX consists of randomly oriented grains.

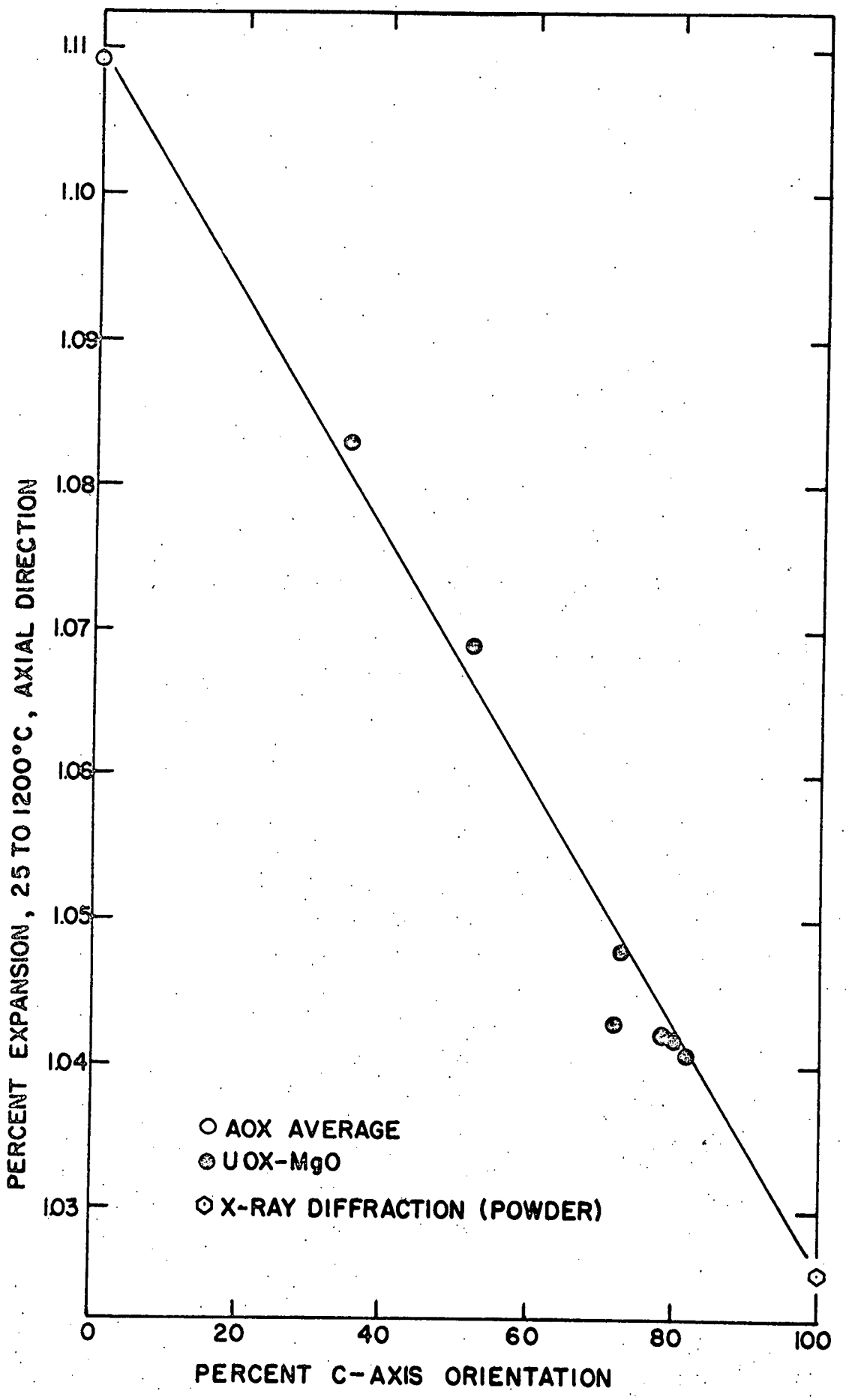
1.11
1.10
1.09
1.08
1.07
1.06
1.05
1.04
1.03
PERCENT EXPANSION, 25 TO 1200°C, AXIAL DIRECTION
AOX AVERAGE
UOX-MgO
X-RAY DIFFRACTION (POWDER)
0
20
40
60
80
100
PERCENT C-AXIS ORIENTATION

Fig. 3

TABLE III

BeO THERMAL EXPANSION ANISOTROPY DEDUCED FROM DILATOMETRIC MEASUREMENTS

Temperature, °C	Linear Expansion From 25 to T°C, %	Expansion of Single Crystal, % (deduced) a axis (1)	c axis (2)	Anisotropy Ratio, % Δ a/% Δ c
	Sample #1, 72% grain orientation (3)			
300	0.174	0.1996	0.1631	1.1073
600	0.429	0.4678	0.4201	1.1135
800	0.613	0.6830	0.5969	1.1442
1000	0.817	0.9147	0.7945	1.1512
1200	1.045	1.1950	1.0170	1.1362
	Sample #2, 52% grain orientation			
300	0.179	0.1969	0.1696	1.1727
600	0.436	0.4673	0.4211	1.1097
800	0.630	0.6778	0.6073	1.1160
1000	0.839	0.9090	0.8057	1.1282
1200	1.069	1.1465	1.0313	1.1136
	Sample #3, 35% grain orientation			
300	0.177	0.2064	0.1545	1.3359
600	0.442	0.4660	0.4236	1.1000
800	0.636	0.6804	0.6020	1.1302
1000	0.847	0.9140	0.7957	1.1486
1200	1.083	1.1471	1.0340	1.1093
	Sample #4, 82% grain orientation			
300	0.179	0.1953	0.1768	1.1046
600	0.428	0.4664	0.4228	1.1031
800	0.612	0.6801	0.6027	1.1284
1000	0.818	0.9091	0.8056	1.1284
1200	1.041	1.1511	1.0260	1.1219
	Sample #5, 73% grain orientation			
300	0.171	0.2015	0.1642	1.2271
600	0.422	0.4725	0.4108	1.1501
800	0.609	0.6855	0.5920	1.1579
1000	0.819	0.9128	0.7961	1.1437
1200	1.048	1.1516	1.0249	1.1236
	Sample #6, 80% grain orientation			
300	0.178	0.1960	0.1753	1.1180
600	0.426	0.4680	0.4196	1.1153
800	0.611	0.6813	0.6003	1.1349
1000	0.815	0.9118	0.8003	1.1393
1200	1.042	1.1514	1.0254	1.1228

TABLE III (Cont.)

BeO THERMAL EXPANSION ANISOTROPY DEDUCED FROM DILATOMETRIC MEASUREMENTS

Temperature, °C	Linear Expansion From 25 to T°C, %	Expansion of Single Crystal, % (deduced) a axis (1)	c axis (2)	Anisotropy Ratio, % Δ a/% Δ c
	Sample #7, 79% grain orientation			
300	0.178	0.1961	0.1751	1.1199
600	0.428	0.4670	0.4216	1.1076
800	0.614	0.6798	0.6033	1.1268
1000	0.819	0.9098	0.8042	1.1313
1200	1.042	1.1521	1.0241	1.1249

(1) Random + $\left[\frac{(\text{random} - \text{observed}) \times 100}{2 \times \% \text{ orientation}}\right]$

(2) Random - $\left[\frac{(\text{random} - \text{observed}) \times 100}{\% \text{ orientation}}\right]$

(3) Preferential c axis grain orientation in the direction of measurement (longitudinal direction of cylindrical specimen).

TABLE IV

SUMMARY OF BeO THERMAL EXPANSION ANISOTROPY

Temperature, °C	Expansion from 25°C, % a axis	Expansion from 25°C, % c axis	Anisotropy Ratio, % Δ a/% Δ c	Mean expansion coefficient from 25°C, 10^{-6} in/in°C a axis	Mean expansion coefficient from 25°C, 10^{-6} in/in°C c axis
X-ray diffraction, powdered sample					
600	0.4633	0.4020	1.1525	8.06	6.99
800	0.6746	0.5985	1.1272	8.70	7.72
1000	0.8896	0.7881	1.1288	9.12	8.08
1200	1.1639	1.0257	1.1347	9.91	8.73
Dilatometric measurements, Table III average					
300	0.1991	0.1691	1.1774	7.24	6.15
600	0.4679	0.4199	1.1142	8.14	7.30
800	0.6811	0.6006	1.1341	8.79	7.75
1000	0.9116	0.8006	1.1387	9.35	8.21
1200	1.1511	1.0261	1.1218	9.80	8.73

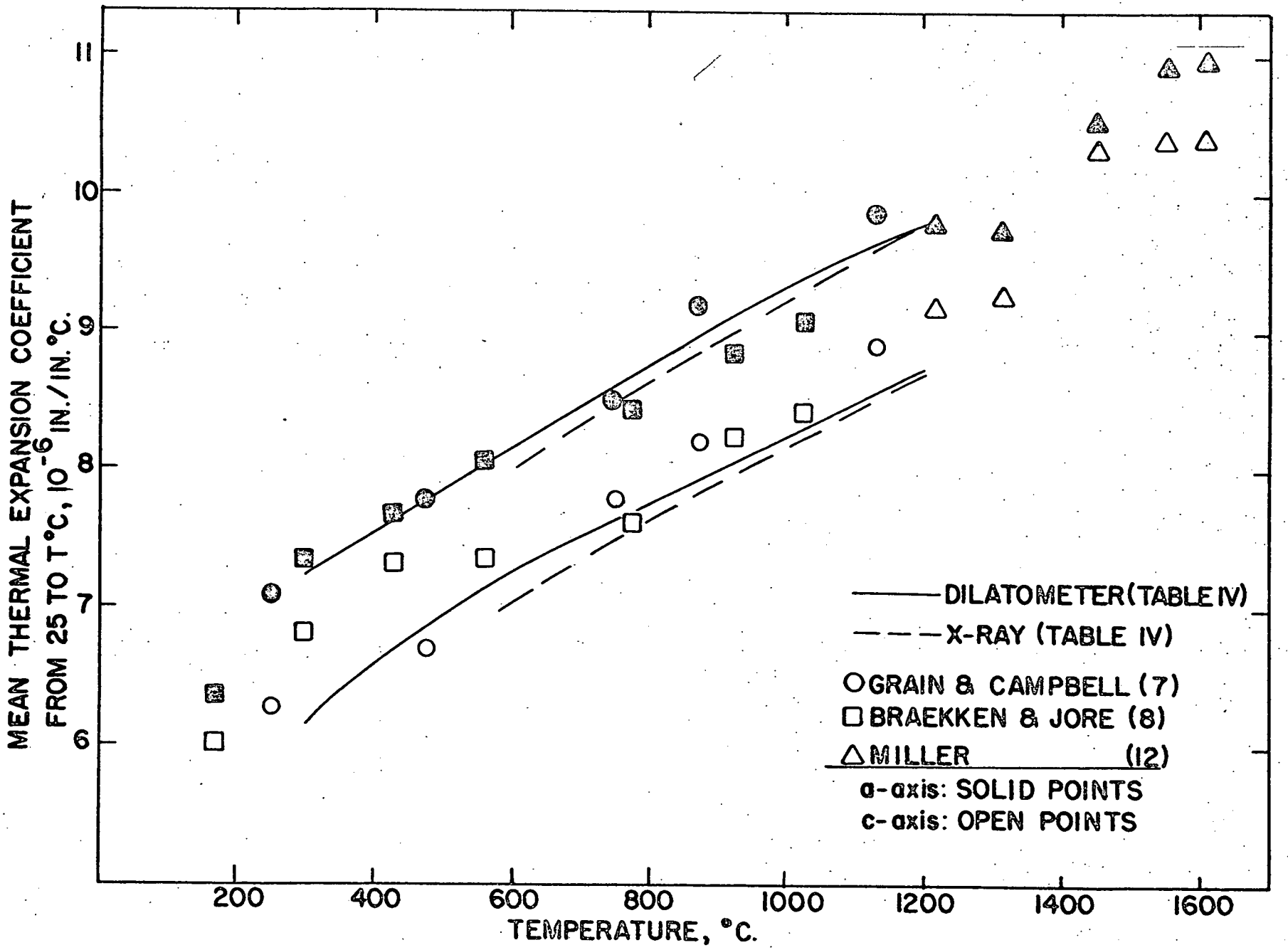
MEAN THERMAL EXPANSION COEFFICIENT
FROM 25 TO T°C, 10^{-6} IN./IN.°C.
11
10
9
8
7
6
200
400
600
800
1000
1200
1400
1600
TEMPERATURE, °C.
DILATOMETER (TABLE IV)
X-RAY (TABLE IV)
GRAIN & CAMPBELL (7)
BRAEKKEN & JORE (8)
MILLER (12)
a-axis: SOLID POINTS
c-axis: OPEN POINTS

Fig. 4

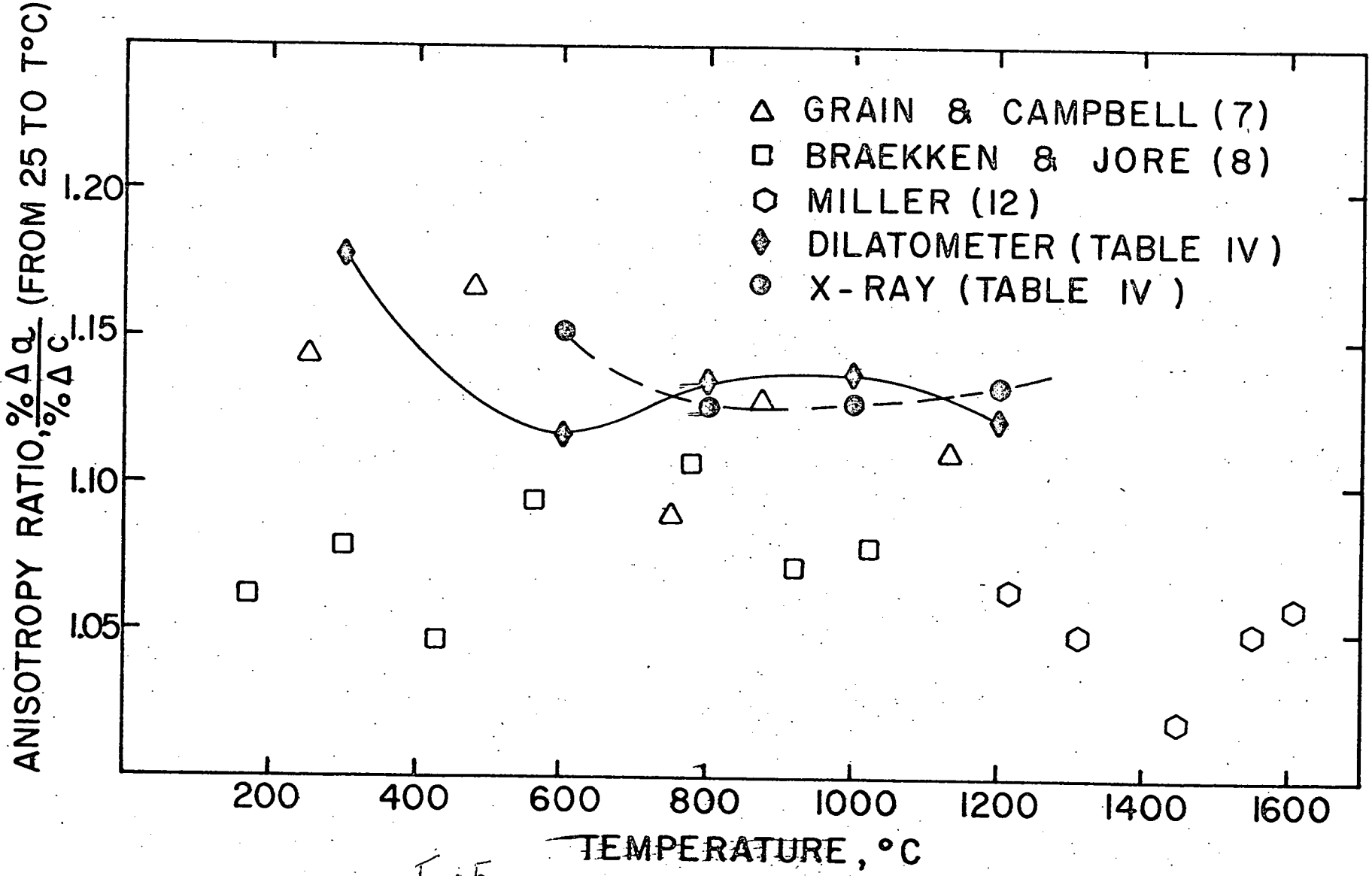
ANISOTROPY RATIO, $\frac{\%\Delta a}{\%\Delta c}$ (FROM 25 TO T°C)
1.20
1.15
1.10
1.05
200
400
600
800
1000
1200
1400
1600
TEMPERATURE, °C
GRAIN & CAMPBELL (7)
BRAEKKEN & JORE (8)
MILLER (12)
DILATOMETER (TABLE IV)
X-RAY (TABLE IV)

Fig 5

III. DYNAMIC ELASTIC CONSTANTS

(1) Methods of Measurement

The dynamic Young's modulus and the shear modulus were calculated from measurements of the fundamental resonance frequencies of round rods, 0.238 inch in diameter and 3.500 inches long. Young's modulus was calculated from the resonance frequency measurement of the flexural mode of vibration and the shear modulus from the torsional mode in accordance with standard equations[13].

For room temperature measurements, the specimens were supported on two fine cross-wires at the nodes of the fundamental flexural mode of vibration. The specimens were vibrated by means of a variable frequency oscillator driving a piezoelectric transducer coupled to one end of the specimen through a fine wire touching the end. The resonance frequencies were monitored by a second piezoelectric transducer coupled to the specimen by means of another fine wire touching the other end of the specimens. The received signal was amplified, displayed on an oscilloscope, and the resonance frequency indicated on an electronic counter having an accuracy of 0.01 percent of the measured frequency. For this specimen size and shape, the fundamental flexural resonance frequency ranged from 6-8 kilocycles per second and the torsional resonance frequency from 35-40 kilocycles per second. The correction to Young's modulus for size, shape, and Poisson's ratio amounted to about 2.5 percent increase above that calculated from the frequency measurement, and was made in accordance with the equations and tables set forth by Spinner and Tefft[13]. Identification of the vibrational modes was made by observation

of the phase shift when traversing the specimen length for the fundamental resonance flexural mode and by traversing the diameter for the torsional mode as discussed by Spinner and Tefft[13].

Three rods selected at random were chosen as standards. These rods have been measured repeatedly to insure against drift in the equipment with time and have served to establish precision limits for the elastic constants measurements. Based upon approximately 100 readings of the standard rods over a period of time, it is concluded that the precision limits are such that at the 95% confidence level, the room temperature Young's modulus for an individual rod is reproducible to within ± 0.26 percent, the shear modulus to within ± 0.49 percent and the calculated Poisson's ratio to within ± 2.1 percent.

For elevated temperature measurements, the specimens were suspended in a tube furnace from two .010 inch platinum wires located near the fundamental flexural nodal points. The driver crystal was attached to one wire and the receiver crystal to the other wire external from the furnace. The same electronic equipment was used for elevated temperature measurements as was used for room temperature measurements. The frequency measurements at 20°C by the two different specimen support methods employed were repeatable within the limits stated for the standard rods.

(2) Experimental Results

Room Temperature Measurements

The dynamic elastic constants were determined at 20°C for extruded AOX

and UOX-MgO over the grain size range of 5-80 microns and the fractional porosity range of 0.02-0.15. The data for the two compositions at each nominal grain size have been fit by the method of least squares to three different porosity equations of the following types:

$$E = E_o \left[1 - bP\right] \tag{3}$$

$$E = E_o \, e^{-bP} \tag{4}$$

$$E = E_o \left[1 + \frac{AP}{1-(A+1)P}\right] \tag{5}$$

where E is the dynamic elastic modulus (Young's or shear) at the fractional porosity, P, and E_o is the elastic modulus at theoretical density, 3.01 g/cm^3.

Equation (3) is a simple linear fit of the data and describes the data sufficiently well for most practical purposes. Equation (4) is an exponential fit of the data proposed by Spriggs,[14] and equation (5) is the semi-theoretical equation of Hasselman[15]. A comparison of results obtained from the three equations is shown in Table V where it can be seen that the standard error of estimate is less for equation (5) of Hasselman than for the other two equations. Equation (5) also extrapolates to zero at a fractional porosity of 1.0. A comparison of results by the three equations for AOX material (randomly oriented) is shown in Figure 6 extrapolated beyond the range of the input data to show the limits of the equations. The results are also compared to a previous survey of the literature that was made by Lillie[16]. Lillie's survey of BeO of various microstructures would indicate a greater dependency on porosity than our own data.

TABLE V

COMPARISON OF EQUATIONS RELATING DYNAMIC YOUNG'S MODULUS TO POROSITY

Range			$E = E_o [1 - bP]$			$E = E_o e^{-bP}$			$E = E_o \left[1 + \frac{AP}{1-(A+1)P}\right]$		
Grain Size, microns	Fraction Porosity	No. Of Observations	E_o 10^6 psi	b	Standard Error, %	E_o 10^6 psi	b	Standard Error, %	E_o 10^6 psi	A	Standard Error, %
UOX-MgO											
2-5	0.04-0.17	150	54.9	1.72	2.34	55.7	2.06	2.35	55.3	-1.99	2.08
7-10	0.02-0.16	150	57.3	1.82	1.19	58.2	2.21	1.35	58.2	-2.24	0.76
15-20	0.02-0.15	150	59.2	1.80	1.09	59.9	2.14	1.28	59.9	-2.16	0.70
35-50	0.02-0.14	150	62.8	2.25	1.86	63.7	2.71	1.77	63.7	-2.81	1.36
AOX											
5-100	0.02-0.15	490	56.1	1.86	1.83	56.7	2.20	1.77	56.6	-2.19	1.27

E_o = the modulus of elasticity at zero porosity, 10^6 psi.

The variation of E_o with grain size in UOX-MgO is caused by an increasing degree of orientation with increasing grain size; it is not a function of grain size per se.

Standard error is the mean error between the observed and calculated values of E in percent.

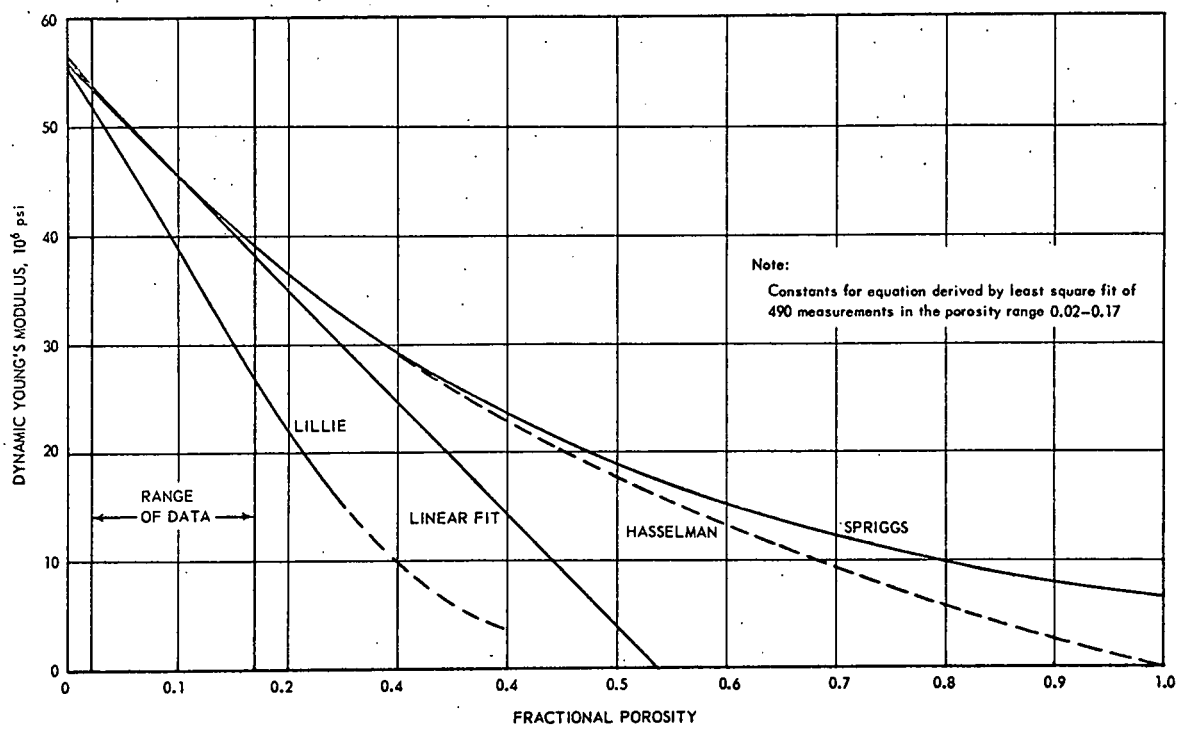
DYNAMIC YOUNG'S MODULUS, 10^6 psi
60
50
40
30
20
10
0
0
0.1
0.2
0.4
0.4
0.5
0.6
0.7
0.8
0.9
1.0
FRACTIONAL POROSITY
Note:
Constants for equation derived by least square fit of 490 measurements in the porosity range 0.02–0.17
LILLIE
RANGE OF DATA
LINEAR FIT
HASSELMAN
SPRIGGS

Fig. 6

As mentioned previously, BeO extruded from UOX material exhibits a degree of preferred grain orientation in extrusion which is enhanced with grain growth during sintering; consequently, the larger the grain size in the sintered body the larger is the percentage of grains having the c-axis oriented in the direction of extrusion. This effect results in higher elastic constants at a given porosity for extruded UOX material as grain size increases. On the other hand, AOX is essentially random in orientation and there is little change in the elastic constants as grain size increases. The best estimate of E as a function of preferred grain orientation in polycrystalline BeO has been obtained from selected specimens of UOX-MgO for which both Young's modulus and orientation distribution functions were measured. The results of measurements made on eleven such specimens are shown in Figure 7 where the Young's modulus values, corrected to zero porosity, are plotted as a function of percent orientation of c-axes with the axis of extrusion, calculated by the method of Sjodahl and Bartram[1]. Corrections to zero porosity for Young's modulus are made according to the equations presented in Table VI.

A summary of Young's and shear moduli data fit to Hasselman's equation (5) is presented in Table VI for the nominal grain sizes of UOX-MgO and AOX investigated. In addition, composite equations for the two moduli are presented for (1) isostatically pressed UOX, isostatically pressed AOX, and hot pressed basic acetate derived BeO (fabricated by Atomics International) all of which are essentially random in grain orientation, and (2) the above randomly oriented bodies and all of the extruded AOX over the grain size range 5-80 microns. The latter equations represent the best estimate of dynamic elastic constants for randomly oriented BeO.

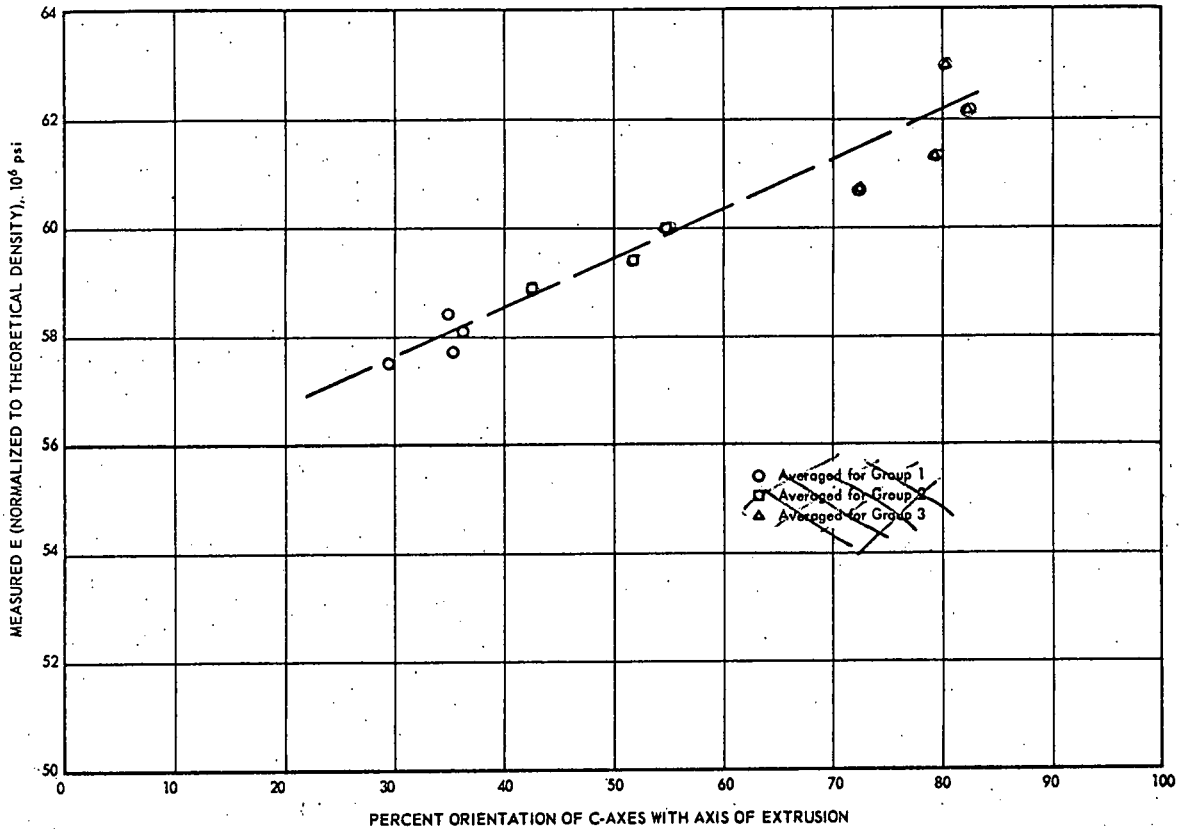
MEASURED E (NORMALIZED TO THEORETICAL DENSITY), 10^6 psi
64
62
60
58
56
54
52
50
0
10
20
30
40
50
60
70
80
90
100
PERCENT ORIENTATION OF C-AXES WITH AXIS OF EXTRUSION
Averaged for Group 1
Averaged for Group 2
Averaged for Group 3

Fig 7

TABLE VI

YOUNG'S AND SHEAR MODULI VS. POROSITY (HASSELMAN EQUATION)

Composition	Fractional Porosity Range	Density Range, g/cm^3	Grain Size, microns	Equation Constants		No. of Observations	Standard Error of Estimate	
		YOUNG'S MODULUS	$E = E_o\left[1 + \frac{AP}{1-(A+1)P}\right]$	E_o	A		%	10^6 psi
UOX + 0.5 wt. % MgO (Extruded)	0.04 - 0.17	2.50 - 2.90	2-5	55.30	-1.99	150	2.08	1.15
	0.02 - 0.16	2.53 - 2.95	7-10	58.24	-2.24	150	0.76	0.44
	0.02 - 0.15	2.56 - 2.94	15-20	59.91	-2.16	150	0.70	0.42
	0.02 - 0.14	2.60 - 2.95	35-50	63.72	-2.61	150	1.36	0.87
	0.02 - 0.10	2.71 - 2.96	60-80	61.08	-2.10	100	2.50	1.53
AOX (Extruded)	0.02 - 0.16	2.55 - 2.95	5-100	56.60	-2.19	490	1.27	0.72
	0.06 - 0.16	2.55 - 2.83	2-5	55.09	-2.12	100	3.07	1.69
	0.03 - 0.16	2.55 - 2.91	7-10	55.82	-2.03	150	0.43	0.24
	0.03 - 0.16	2.54 - 2.91	15-20	57.07	-2.22	150	0.21	0.12
	0.02 - 0.14	2.60 - 2.96	35-50	57.28	-2.32	150	0.56	0.32
	0.02 - 0.09	2.73 - 2.96	60-80	55.85	-2.10	100	0.93	0.52
Composite of Random Material	0.00 - 0.16	2.55 - 3.00	5-80	56.42	-2.19	786	0.99	0.56
UOX, AOX, HPA[a] (Isostatic and Hot Press)	0.00 - 0.06	2.83 - 3.00	20-40	56.55	-2.33	136	0.26	0.15
		SHEAR MODULUS	$G = G_o\left[1 + \frac{AP}{1-(A+1)P}\right]$	G_o	A			
UOX + 0.5 wt. % MgO (Extruded)	0.04 - 0.17	2.50 - 2.90	2-5	21.04	-2.00	150	0.57	0.12
	0.02 - 0.16	2.53 - 2.95	7-10	22.01	-2.28	150	0.27	0.06
	0.02 - 0.15	2.56 - 2.94	15-20	22.75	-2.28	150	0.22	0.05
	0.02 - 0.14	2.60 - 2.95	35-50	23.90	-2.80	150	0.46	0.11
	0.02 - 0.10	2.71 - 2.96	60-80	23.16	-2.31	100	0.73	0.17
AOX (Extruded)	0.06 - 0.16	2.55 - 2.83	2-5	20.93	-2.13	100	1.10	0.23
	0.03 - 0.16	2.55 - 2.91	7-10	21.23	-2.12	150	0.19	0.04
	0.03 - 0.16	2.54 - 2.91	15-20	21.61	-2.20	150	0.42	0.09
	0.02 - 0.14	2.60 - 2.96	35-50	21.78	-2.33	150	0.18	0.04
	0.02 - 0.09	2.73 - 2.96	60-80	21.22	-2.14	100	0.33	0.07
Composite of Random Material	0.00 - 0.16	2.55 - 3.00	5-80	21.45	-2.22	786	0.04	0.10
UOX, AOX, HPA[a] (Isostatic and Hot Press)	0.00 - 0.06	2.83 - 3.00	20-40	21.68	-2.75	136	0.14	0.03

(a) HPA = BeO derived from basic acetate.

Inspection of the values for E_o and G_o for both UOX-MgO and AOX in Table VI reveal rather low values in the 2-5 micron range and a drop-off in the 60-80 micron range. It is known that the small grain size material (2-5 micron) contained mostly intergranular porosity of different size, shape, and distribution than specimens of larger grain size which could account for the difference in porosity dependence. Spriggs[14] has discussed the effect of different forms of porosity on the elastic constants (60-100 microns). In the larger grain size specimens, intragranular cracks were observed, increasing in number and severity in the 100 micron grain size range to a point where it was sometimes impossible to measure the elastic constants.

Elevated Temperature Measurements

Young's modulus and the shear modulus as a function of temperature were determined for representative samples of the various grain sizes and densities up to 1400°C. No consistent trends with grain size, density, or preferred grain orientation were apparent and the data from both AOX and UOX-MgO specimens covering the entire grain size - density range were combined for a statistical least square fit of the data in terms of percent decrease in either Young's modulus (E) or the shear modulus (G) from the 20°C values presented in Table VI. The following equations indicate the percent decrease from the 20°C value in the elastic constants E and G with temperature in the range 20 to 1400°C.

$$\% \text{ Decrease in } E = 8.83 \times 10^{-3} (T-20) + 1.29 \times 10^{-9} (T-20)^3 \quad (6)$$

$$\% \text{ Decrease in } G = 8.80 \times 10^{-3} (T-20) + 1.66 \times 10^{-9} (T-20)^3 \quad (7)$$

The standard errors of estimate for the individual points about the calculated lines are ± 1.15 percent decrease for E and ± 1.70 percent decrease for G. The larger standard error of estimate for G results from a greater difficulty in measuring the torsional vibrational mode, especially at elevated temperatures. A comparison of curves plotted from equations 6 and 7 is made in Figure 8 to summary curves presented by Lillie[16] in which he compares data obtained by Atomics International and Argonne National Laboratory. It can be seen that all data are in quite good agreement. There apparently is little if any real difference in the temperature dependence of E and G and from a practical point of view either equation (6) or (7) adequately describes the behavior of both constants.

(3) Discussion of Results

When it was observed that the degree of preferred grain orientation had such a large effect on Young's modulus, it was concluded that the polycrystalline Young's modulus data, obtained from UOX-MgO rods over a wide range of grain size, could be used in conjunction with orientation distribution functions to deduce some of the compliance moduli for single crystals of BeO. This appeared to be possible since in a polycrystalline body, Young's modulus is reasonably well represented by the space average of the individual crystal E's in the direction of measurement[17]. Consequently, the eleven rods for which orientation distribution functions were determined, those presented in Figure 7, were used to establish an equation for Young's modulus of single BeO crystals as a function of the angle of measurement from the c-axis[18]. The resulting equation,

$$\frac{1}{E_\theta} = 0.0178 \sin^4\theta + 0.0151 \cos^4\theta + 0.0410 \sin^2\theta \cos^2\theta \qquad (8)$$

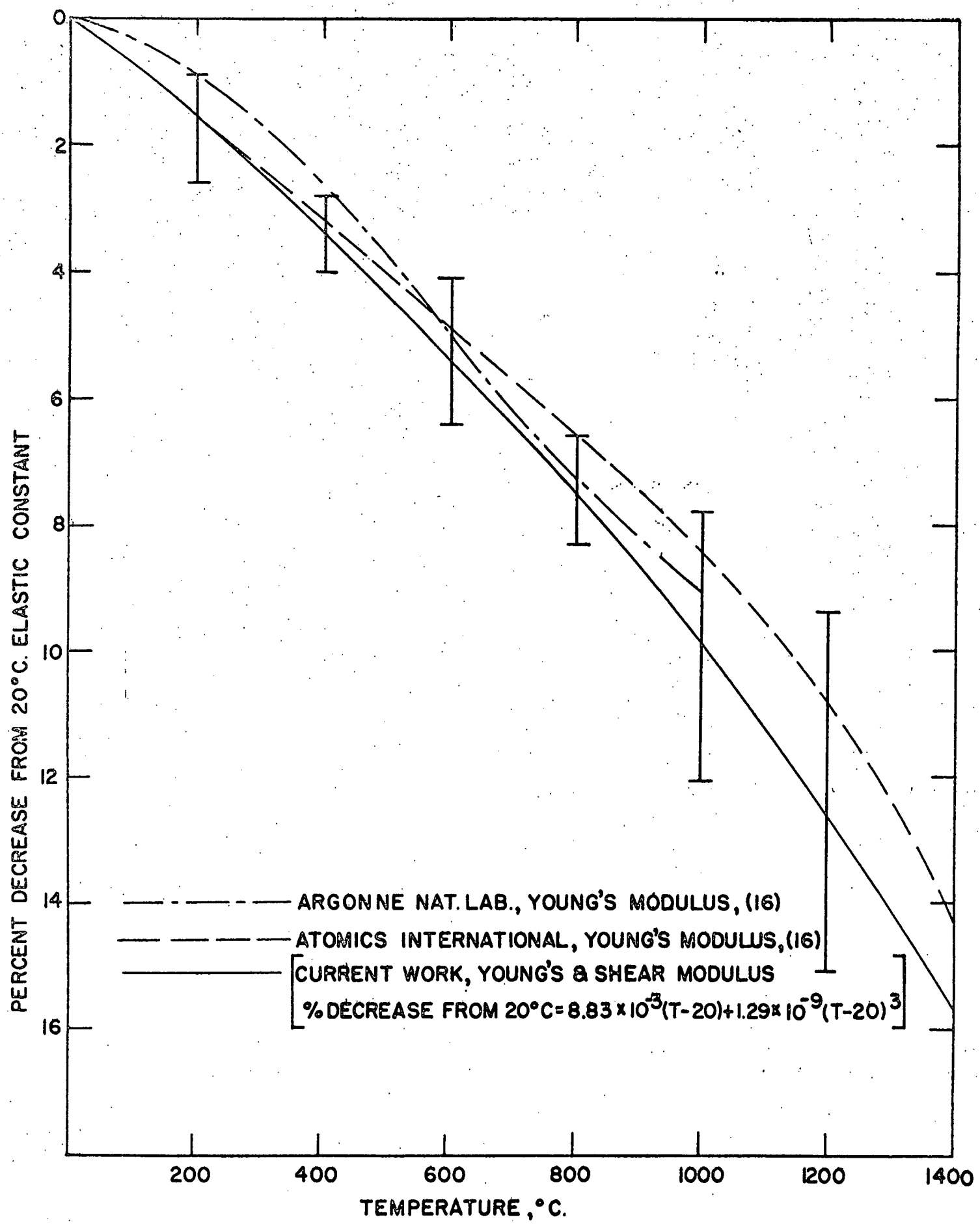
PERCENT DECREASE FROM 20°C. ELASTIC CONSTANT
0
2
4
6
8
10
12
14
16
200
400
600
800
1000
1200
1400
TEMPERATURE, °C.
ARGONNE NAT. LAB., YOUNG'S MODULUS, (16)
ATOMICS INTERNATIONAL, YOUNG'S MODULUS, (16)
CURRENT WORK, YOUNG'S & SHEAR MODULUS
% DECREASE FROM 20°C = 8.83 x 10^-3 (T-20) + 1.29 x 10^-9 (T-20)^3

Fig 8

where E_θ is Young's modulus in 10^6 psi measured at the angle θ from the c-axis, predicts a value for E of 66.2 x 10^6 psi in the direction of the c-axis and 56.1 x 10^6 psi in the direction of the a-axes. These values lead to an anisotropy ratio E_a/E_c of 0.85 for Young's modulus. Equation 8 is plotted as Figure 9 along with two reference curves for cadmium sulfide (same space group, C_{6v}, as BeO) which were normalized to the BeO curve for comparision of curve shape. The CdS curves, were plotted from data obtained by Berlincourt[19] and Bolef[20], et.al., from measurements of CdS single crystals. A single point representing a measurement of a single crystal of BeO made by Austerman, et.al.[21], in the basal plane is also shown for comparison and is higher than the value for the basal plane predicted from equation 8. It is believed that the calculated value of the c-axis Young's modulus for single crystals is quite good since the calculation of the equation was obtained from rods having preferred orientation of the c-axis in the direction of extrusion ranging from 30 to 80 percent. The value for the a-axes is not as reliable but it is obvious from the measurements that Young's modulus is less in the plane of the a-axes than in the direction of the c-axis, and that a minimum occurs between the two extremes. A maximum crystal anisotropy of about 0.8 for E_θ/E_c is predicted from equation 8 when θ equals about 55°.

A large discrepancy exists in the calculated values of Poisson's ratio for BeO between measurements reported by Bentle[22] and our data when calculated from the well known equation:

$$\nu = \left(\frac{E}{2G} - 1\right) \qquad (9)$$

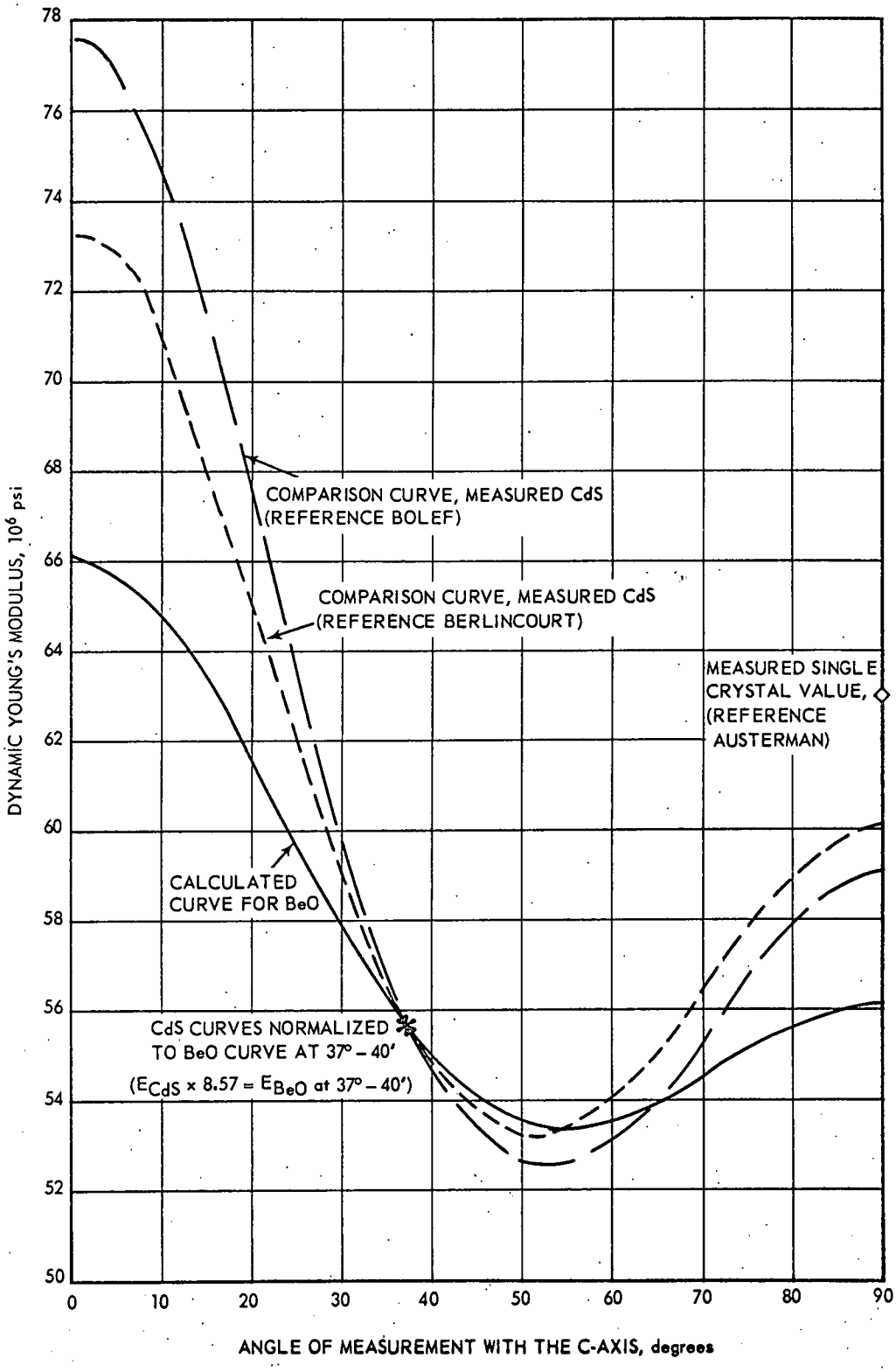
78
76
74
72
70
68
66
64
62
60
58
56
54
52
50
0
10
20
30
40
50
60
70
80
90
DYNAMIC YOUNG'S MODULUS, 10^6 psi
ANGLE OF MEASUREMENT WITH THE C-AXIS, degrees
COMPARISON CURVE, MEASURED CdS (REFERENCE BOLEF)
COMPARISON CURVE, MEASURED CdS (REFERENCE BERLINCOURT)
MEASURED SINGLE CRYSTAL VALUE, (REFERENCE AUSTERMAN)
CALCULATED CURVE FOR BeO
CdS CURVES NORMALIZED TO BeO CURVE AT 37° – 40'
($E_{CdS} \times 8.57 = E_{BeO}$ at 37° – 40')

Fig. 9

Bentle reports values for Poisson's ratio in the neighborhood of 0.20 for BeO whereas calculated Poisson's ratios based upon the equations presented in Table VI predict values of 0.3 or greater. It is known that Poisson's ratio calculated by means of equation 9 is an approximation and applies only to isotropic bodies. However, in a polycrystalline body composed of anisotropic crystals a random distribution of these crystals constitutes an isotropic condition on a macroscopic scale[13]. Therefore, Poisson's ratio for the randomly oriented material, extruded AOX or isostatically pressed material, should be approximately correct if the proper values for Young's modulus and the shear modulus are used in equation 9. The advisability of using equation 9 to predict Poisson's ratio in preferentially oriented bodies composed of anisotropic crystals is debatable and subject to an unknown amount of error. The largest chance for error in the resonance frequency technique is in the possible mistaken identity of a resonance peak. For example, it could be possible to mistakenly identify the second overtone of the flexural fundamental frequency as the torsional frequency since both are within 2,000 cycles for the specimen size and shape that was used. However, the second overtone appears at a fixed ratio above the fundamental and it was possible by using the technique described by Spinner and Tefft[13] to identify the particle motion both for the second overtone of the flexural vibrational mode, and the torsional mode fundamental frequency. Since both the equations for Young's modulus and the shear modulus are very accurate for round specimens having a large L/D ratio when the Young's modulus is corrected for size and shape of the specimen, there is every reason to believe that the value for Poisson's ratio in randomly oriented BeO is as accurate as equation 9 permits and that the best estimate of this calculated value is 0.315.

IV. MODULUS OF RUPTURE

(1) Method of Measurement

Modulus of rupture measurements were made using the standard cylindrical rod specimen previously discussed. All measurements reported are 4-point loading over a 3-inch span with a constant moment over the middle one inch (frequently referred to as third point loading). A constant loading head travel rate of 0.05 inch per minute was used.

(2) Experimental Results

The average modulus of rupture strength for the nominal grain sizes and densities of AOX and UOX-MgO are shown in Table VII as well as the number of specimens ruptured, and the standard deviation for the individual measurements about the mean value for the six measurement temperatures, 20, 300, 500, 800, 1000, and 1200°C. The nominal grain sizes and densities for the rods are also shown. An inspection of Table VII shows that there is a wide variation in the standard deviation of different microstructures but the mode lies between 3,000 and 4,000 psi indicating a rather large scatter in sample strengths about the mean values. The data of Table VII are further summarized in Table VIII where the room temperature strength data for each microstructure is given and the elevated temperature data presented in terms of the fractional room temperature strength.

(3) Discussion of Results

Inspection of Table VIII reveals several interesting trends. First, it will be noted that for a given composition-density combination, the room temperature strength increases as expected with decreasing grain size with the exception of the 5 micron grain size material which shows a decrease

TABLE VII

SUMMARY OF MODULUS OF RUPTURE VALUES FOR BeO[a]

Composition	Nominal Grain Size, microns	Nominal Density, g/cm³	20°C Modulus of Rupture N[b]	20°C X̄[c]	20°C S_x[d]	300°C N	300°C X̄	300°C S_x	500°C N	500°C X̄	500°C S_x
UOX-MgO	100	2.90	15	16.6	1.99	6	18.3	1.56	7	21.8	1.38
	80	2.90	19	18.2	4.75	9	26.6	3.32	9	21.8	2.66
	50	2.90	28	23.3	2.61	15	24.0	3.66	15	25.3	2.96
	20	2.90	40	31.7	3.81	15	31.3	5.74	15	34.7	3.87
	10	2.90	19	32.4	4.13	7	32.8	6.26	8	35.9	3.66
	5	2.90	21	30.7	4.19	15	27.6	5.32	15	29.6	5.51
	80	2.75	30	18.0	1.74	15	20.7	3.33	15	18.4	1.97
	50	2.75	10	17.0	2.21	6	21.7	3.03	6	18.0	1.11
	20	2.75	15	25.8	4.30	15	27.0	3.91	15	26.5	2.25
	10	2.75	10	35.6	3.32	6	31.3	6.41	7	32.5	4.25
	5	2.75	13	30.3	4.18	15	32.1	4.44	15	32.7	4.14
	50	2.60	17	17.7	1.10	15	17.9	2.33	15	18.1	2.59
	20	2.60	13	25.5	1.78	14	19.9	1.06	14	24.4	2.91
	10	2.60	10	28.2	2.09	1	31.2	-	-	-	-
	5	2.60	30	31.1	3.35	15	31.0	3.06	15	31.2	4.60
AOX	100	2.90	30	12.1	2.27	15	14.8	2.60	15	13.5	3.07
	80	2.90	17	15.4	0.83	7	16.9	3.46	7	17.2	3.67
	50	2.90	41	19.3	2.05	18	20.7	7.29	19	20.1	2.98
	20	2.90	62	34.1	3.49	15	35.1	5.19	15	34.9	3.54
	10	2.90	20	33.3	3.85	8	38.2	5.57	12	33.6	3.23
	80	2.75	15	14.4	1.05	4	12.8	-	3	19.8	-
	50	2.75	15	20.2	3.11	4	21.7	-	3	27.4	-
	20	2.75	30	27.8	2.14	16	29.2	2.81	15	30.1	2.63
	10	2.75	14	34.1	2.72	7	35.7	3.76	8	38.8	4.41
	5	2.75	14	26.0	3.59	3	31.7	-	4	37.3	-
	50	2.60	14	18.1	0.91	12	16.1	2.85	10	15.7	5.69
	20	2.60	30	23.8	5.02	15	23.3	5.02	15	24.1	2.43
	10	2.60	30	29.7	2.98	15	30.4	2.74	15	33.2	3.54
	5	2.60	18	26.9	4.30	5	27.1	-	6	29.0	2.62

Composition	Nominal Grain Size, microns	Nominal Density, g/cm³	800°C Modulus of Rupture N	800°C X̄	800°C S_x	1000°C N	1000°C X̄	1000°C S_x	1200°C N	1200°C X̄	1200°C S_x
UOX-MgO	100	2.90	6	22.2	1.49	7	21.0	2.13	6	23.7	2.80
	80	2.90	9	30.4	3.55	8	33.4	2.14	10	31.2	3.89
	50	2.90	14	25.7	3.45	13	28.1	3.38	14	27.0	2.61
	20	2.90	15	39.9	5.81	16	34.8	3.75	15	28.4	2.30
	10	2.90	8	33.9	4.70	7	33.6	6.17	7	33.8	5.29
	5	2.90	15	28.9	4.70	15	27.1	5.51	15	28.7	6.09
	80	2.75	15	25.5	3.64	15	22.8	2.27	12	25.6	2.38
	50	2.75	6	23.9	3.97	6	22.2	1.54	6	22.3	1.75
	20	2.75	15	30.8	2.84	14	28.9	2.84	15	24.5	2.34
	10	2.75	7	39.3	4.81	7	33.3	5.82	9	31.5	3.54
	5	2.75	15	31.6	3.12	15	33.4	3.18	15	29.6	2.98
	50	2.60	15	20.1	2.07	15	20.8	2.32	14	19.0	2.60
	20	2.60	14	28.2	3.08	14	25.7	2.85	15	18.8	1.89
	10	2.60	1	31.5	-	1	28.1	-	1	29.3	-
	5	2.60	14	34.9	5.01	15	30.8	3.68	14	27.2	5.48
AOX	100	2.90	15	19.1	3.24	15	17.8	2.82	15	17.8	3.42
	80	2.90	8	22.7	2.09	6	20.6	2.16	8	22.7	3.97
	50	2.90	19	25.1	3.35	18	25.0	2.24	19	22.9	2.88
	20	2.90	16	33.8	4.83	15	25.3	3.72	15	20.3	3.35
	10	2.90	11	31.3	6.06	12	23.6	4.60	12	18.8	2.77
	80	2.75	2	15.6	-	4	20.8	-	5	19.7	-
	50	2.75	3	28.2	-	3	28.3	-	4	17.8	-
	20	2.75	15	28.9	4.01	15	27.2	2.32	14	21.4	3.05
	10	2.75	7	33.6	2.47	8	27.4	4.30	10	22.3	1.92
	5	2.75	2	32.1	-	4	21.8	-	2	19.5	-
	50	2.60	9	19.7	1.85	13	18.8	2.78	15	18.0	3.43
	20	2.60	15	23.8	3.96	15	20.4	4.26	15	17.0	3.14
	10	2.60	15	30.8	3.88	14	24.6	5.18	15	18.2	2.34
	5	2.60	7	24.5	4.41	5	21.4	-	6	16.6	3.67

Notes:

(a) 4 point, 3 inch span, 1 inch constant moment, 0.06 in/min head travel.

(b) N = Number of samples.

(c) $\bar{X}$ = Average modulus of rupture of N samples, 10^3 psi.

(d) S_x = Standard deviation of points about the average value, 10^3 psi.

FRACTION OF ROOM TEMPERATURE MODULUS OF RUPTURE [illegible]

Grain Size, microns	Room Temp. M.R., 10^3 psi	No. of Specimen at Each Temp.	800°C	900°C	1000°C	1100°C	1200°C
UOX-MgO, 2.90 gm/cm^3							
100	[illegible]	7	1.10	1.11	[illegible]	[illegible]	1.43
80	14.2	9	1.43	1.20	[illegible]	[illegible]	1.71
50	29.3	15	1.03	1.08	1.10	1.10	1.10
20	31.7	15	0.99	1.09	1.20	1.10	0.90
10	32.4	7	1.01	1.11	1.07	1.04	1.03
5	30.7	15	0.90	0.95	0.94	0.98	0.93
UOX-MgO, 2.75 gm/cm^3							
80	16.0	15	1.19	1.02	1.42	1.27	1.42
50	17.0	6	1.26	1.06	1.40	1.32	1.31
20	29.8	15	1.03	1.03	1.19	1.12	0.93
10	33.8	7	0.88	0.91	1.10	0.94	0.88
5	30.3	15	1.06	1.02	1.04	1.10	0.98
UOX-MgO, 2.60 gm/cm^3							
50	17.7	15	1.01	1.02	1.14	1.16	1.07
20	25.5	15	0.78	0.96	1.10	1.01	0.74
10	28.2	1	1.11	-	1.12	1.00	1.04
5	31.1	15	1.00	1.00	1.12	0.99	0.87
AOX, 2.90 gm/cm^3							
100	12.1	15	1.22	1.12	1.38	1.47	1.47
80	15.4	7	1.10	1.12	1.47	1.34	1.47
50	19.3	18	1.07	1.04	1.30	1.29	1.19
20	34.1	15	1.03	1.02	1.02	0.74	0.60
10	33.3	12	1.15	1.01	0.94	0.71	0.56
AOX, 2.75 gm/cm^3							
80	14.4	5	0.69	1.37	1.06	1.34	1.37
50	20.2	4	1.07	1.36	1.40	1.40	0.88
20	27.8	15	1.05	1.06	1.04	0.96	0.77
10	34.1	8	1.06	1.14	0.96	0.80	0.69
5	25.0	4	1.22	1.43	1.29	0.84	0.75
AOX, 2.60 gm/cm^3							
50	14.1	12	0.89	0.87	1.09	1.04	0.99
20	23.5	15	0.96	1.01	1.00	0.86	0.72
10	29.7	15	1.02	1.12	1.04	0.93	0.81
5	26.9	6	1.01	1.06	0.91	0.80	0.62

Numbers underlined are maxima.

in strength from the 10 micron grain sizes. This difference in behavior of the 5 micron grain size material has appeared in the elastic constants, and in compressive creep measurements as well as in modulus of rupture measurements. This anomalous behavior as mentioned before is attributed to a different distribution, shape, and size of porosity compared to the other grain sizes because of incomplete sintering. Thermal soak tests for 500 hours have shown the 5 micron grain size material shrinks considerably at 1200°C without appreciable grain growth indicating that intergranular pores are closing while all other microstructures appear to be stable under these conditions.

Another trend that can be seen in Table VIII is that the peak strength (values underlined) occur at lower temperatures as grain size decreases. In addition, it will be observed that generally speaking the strength behavior with temperature can be grouped by small, medium, and large grain size for each of the composition-density combinations. That is, the 5, 10, and 20 micron grain size material behaves in a similar manner for all porosities, while the 50 micron grain size material behaves in a different manner, and the 80 and 100 micron grain size material behave in still a different manner. The strength dependencies with temperature grouped as above are shown in Figure 10 where the ratio of the strength at elevated temperatures is shown as a function of temperature for the three sub-divisions of material, small, medium, and large grain sizes disregarding the porosity variable. It will be seen that the strength increase from 20°C to 800°C is greater with increasing grain size. This observation is in agreement with Coble[23] who states that internal stresses at room temperature are greater for larger grain sizes and relax as the temperature approaches the stress free temperature

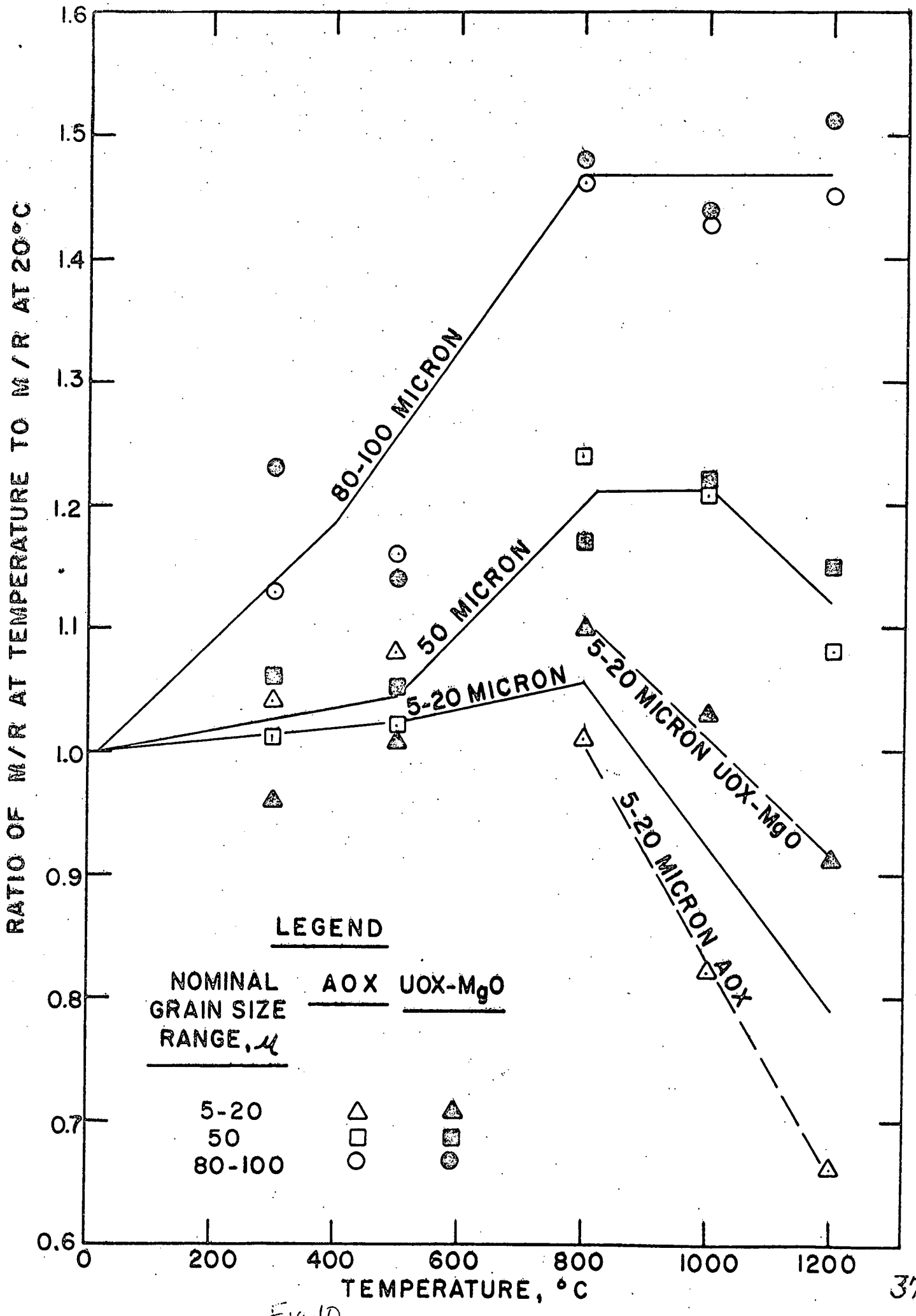
RATIO OF M/R AT TEMPERATURE TO M/R AT 20°C
TEMPERATURE, °C
1.6
1.5
1.4
1.3
1.2
1.1
1.0
0.9
0.8
0.7
0.6
0
200
400
600
800
1000
1200
80-100 MICRON
50 MICRON
5-20 MICRON
5-20 MICRON UOX-MgO
5-20 MICRON AOX
LEGEND
NOMINAL GRAIN SIZE RANGE, μ
AOX
UOX-MgO
5-20
50
80-100

Fig 10

(sintering temperature). At temperatures above 300°C, apparently inelastic strain occurs which causes a reduction in the modulus of rupture. The reduction is larger as the grain size decreases and in the small grain sizes, a difference in inelastic behavior is seen between AOX and UOX-M_gO. This difference between AOX and UOX-M_gO observed at the lower grain sizes and not at the higher could be related to the modulus of rupture loading rate. It is possible that for the loading rate used the inelastic deformation of the small grain size material is fast enough to show a difference between materials while the inelastic deformation rate of the larger grain size material is too slow to permit observation of the material differences.

The data of Table VIII are plotted on an absolute scale in Figure 11 to show the effect of orientation in the temperature range 25 to 300°C. It can be seen that in this temperature range there is little if any real difference in strength between the randomly oriented AOX and the preferentially oriented UOX-MgO for grain sizes up to and including 30 micron. However, there is a significant difference between the preferentially oriented UOX-MgO and the randomly oriented AOX in the 50-100 micron grain size range with the UOX-MgO showing consistently about a 30 percent higher strength. Perhaps it is necessary for the degree of preferred orientation to reach some minimum value before a significant increase in strength can be observed because of the large standard deviation in material strength or because of the relatively insensitive modulus of rupture measurement. The preferred orientation of grains having the crystallographic c-axis oriented with the axis of extrusion in UOX-M_gO approaches 90 percent for grain sizes of about 20 micron, 60-65 percent

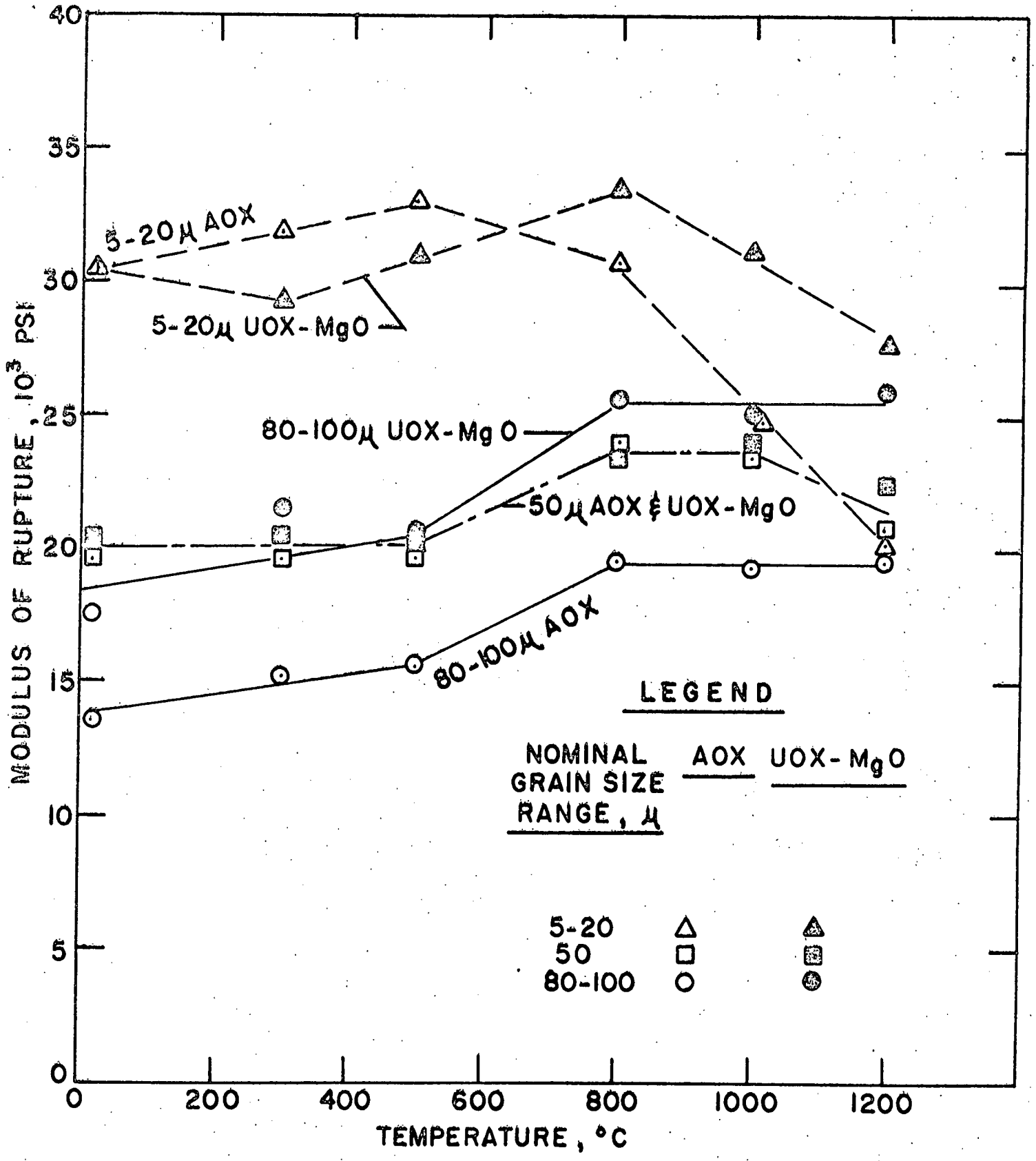
MODULUS OF RUPTURE, 10^3 PSI
TEMPERATURE, °C
0
5
10
15
20
25
30
35
40
0
200
400
600
800
1000
1200
5-20μ AOX
5-20μ UOX-MgO
80-100μ UOX-MgO
50μ AOX & UOX-MgO
80-100μ AOX
LEGEND
NOMINAL GRAIN SIZE RANGE, μ
AOX
UOX-MgO
5-20
50
80-100

Fig 11

for 50 micron grain size, and 80 percent or greater in the 80-100 micron range.

The modulus of rupture data for UOX-MgO and AOX have also been analyzed by fitting the data to the Knudsen equation[24] for grain sizes of 10 microns or greater. The nominal 5 micron material was not included since the strength of the material as pointed out previously was considerably less than would be predicted with the Knudsen correlation. For these correlations, the individual rod modulus of rupture, the grain size by lineal analysis determined for the sinter batch, and the average batch density were used to determine the least square fit of the data for each test temperature to the equation:

$$\ln S = \ln k - a \ln G - bP \qquad (10)$$

which is the logarithmic form of Knudsen's equation,

$$S = k G^{-a} e^{-bP} \qquad (11)$$

where S = modulus of rupture (4 pt, 3 in. span), 10^3 psi

G = grain size by lineal analysis, microns

P = fractional porosity (total) based upon 3.01 g/cm^3 theoretical density

Table IX shows the results of the curve fitting for AOX and for UOX-MgO at each temperature investigated. In addition, the table shows the number of samples used in each correlation, the applicable range of porosity and grain size, correlation coefficients to indicate the degree of correlation of each independent variable to the dependent variable, the 95 percent confidence

TABLE IX

CORRELATION OF MODULUS OF RUPTURE DATA[a] WITH KNUDSEN EQUATION

$$S = k\, G^{-a} e^{-bP}$$

Rupture Temperature, °C	No. of Samples	k	a	b	Average Grain Size, microns	95% Confidence Limits for S, % (b)	(c)
UOX + 0.5 w/o MgO							
20	239	87.7	.35	2.18	28	± 2.7	± 30.8
300	124	65.3	.24	2.31	31	3.9	39.4
500	126	87.8	.31	3.57	30	2.8	28.5
800	125	76.4	.23	2.85	28	3.4	37.1
1000	123	64.0	.19	2.97	30	3.0	34.2
1200	125	49.4	.11	4.25	29	2.9	32.3
AOX							
20	318	14.2	.50	2.51	26	1.6	28.9
300	136	14.2	.49	2.95	26	3.7	46.3
500	137	11.3	.44	1.54	25	3.1	39.3
800	135	75.7	.28	2.32	25	3.1	36.0
1000	138	41.7	.15	1.52	26	3.7	43.0
1200	148	23.9	.03	1.44	26	3.1	41.2

(a) 4 point, 3 inch span, 0.06 in/min head travel.
S = M/R, 10^3 psi; G = lineal grain size microns (range: 7-100 microns);
P = fractional porosity, (range: 0.01-0.15).

(b) 95% confidence limits for the mean value of M/R at the average grain size. The limits at the ends of the applicable grain size range are approximately twice the value shown for the average grain size.

(c) 95% confidence limits within which 95% of measured values would be expected to fall.

limits for the line, and the 95 percent confidence limits for the scatter of individual points about the line. Although the scatter of the points about a line (e.g., S vs G at constant porosity) are quite large as seen in the last column of the table, a sufficiently large number of samples have been tested to narrow the 95 percent confidence limits of a least square line to a reasonable level. These limits, assuming a normal distribution for each grain size - density group, would be those within which the true mean value of modulus of rupture would be expected to fall as a function of grain size for a given porosity, or as a function of porosity for a given grain size. However, the distribution of the modulus of rupture strengths was not normal, but rather skewed and irregular which adds a degree of uncertainty to the statistical results. Figure 12 is a log-log plot of modulus of rupture strength as a function of grain size plotted from the Knudsen correlation for UOX-MgO at 20°C rupture temperature for the three nominal porosities, 3.7, 8.6, and 13.6 percent. The narrow limits about the 3.7 percent porosity line are the calculated 95 percent confidence limits on that line. The points are the average values, taken from Table VII, for the five grain size groups of 2.90 gm/cm^3 nominal density (.037 fractional porosity) to compare to the calculated line. It is clear that 3 of the 5 points fall somewhat outside of the 95 percent limits although from the statistics it would be predicted that all should be within. The outer dashed lines are the limits at 95 percent confidence within which 95 percent of any measured modulus of rupture would be expected to fall for rods having 3.7 percent porosity.

Figure 13 shows the individual Knudsen equation constants, "k", "a", and "b", as a function of temperature for the two grades of material, and

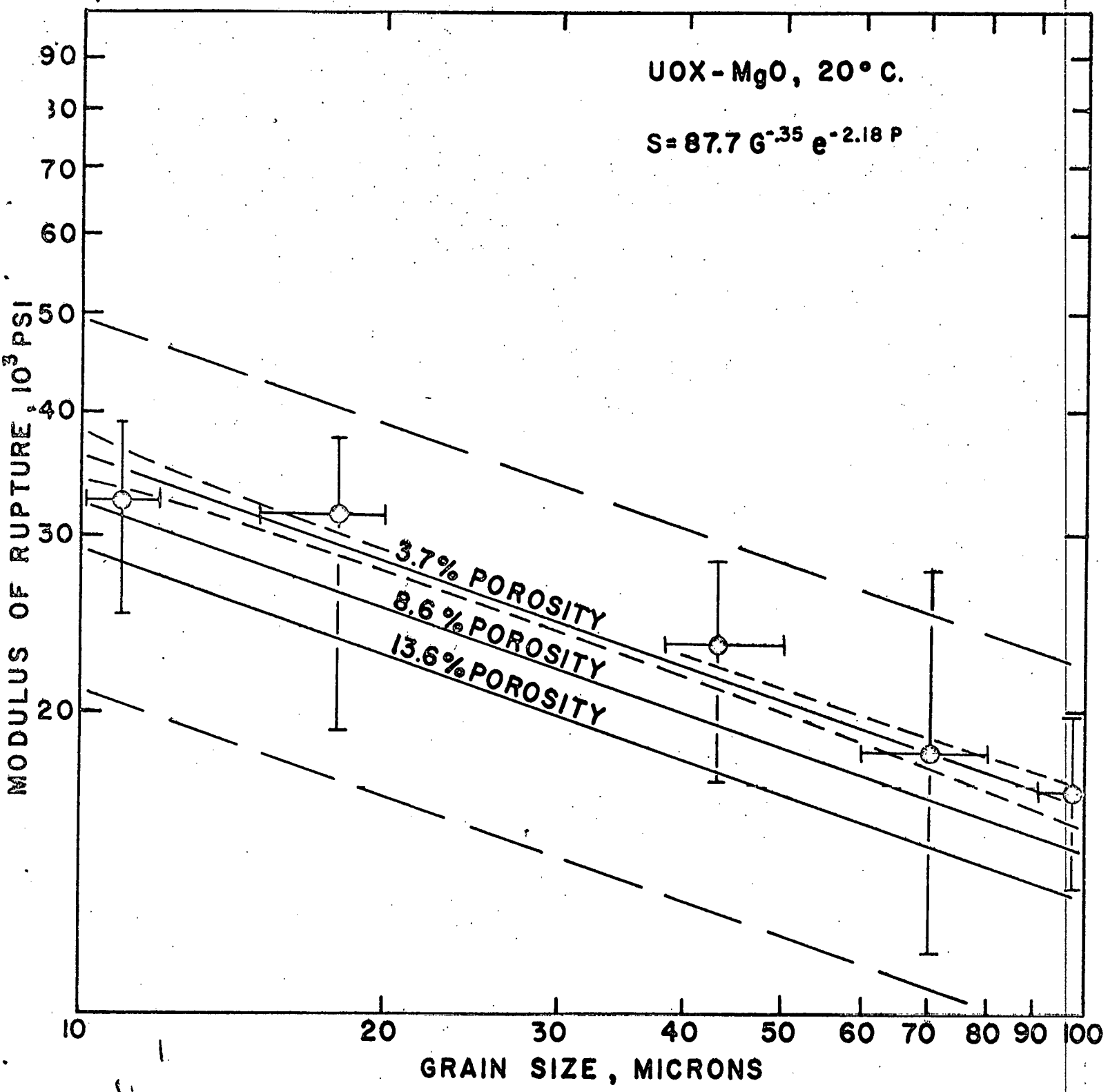
UOX - MgO, 20° C.
S = 87.7 G^-.35 e^-2.18 P
MODULUS OF RUPTURE, 10^3 PSI
90
80
70
60
50
40
30
20
3.7% POROSITY
8.6% POROSITY
13.6% POROSITY
10
20
30
40
50
60
70
80
90
100
GRAIN SIZE, MICRONS

Fig 12

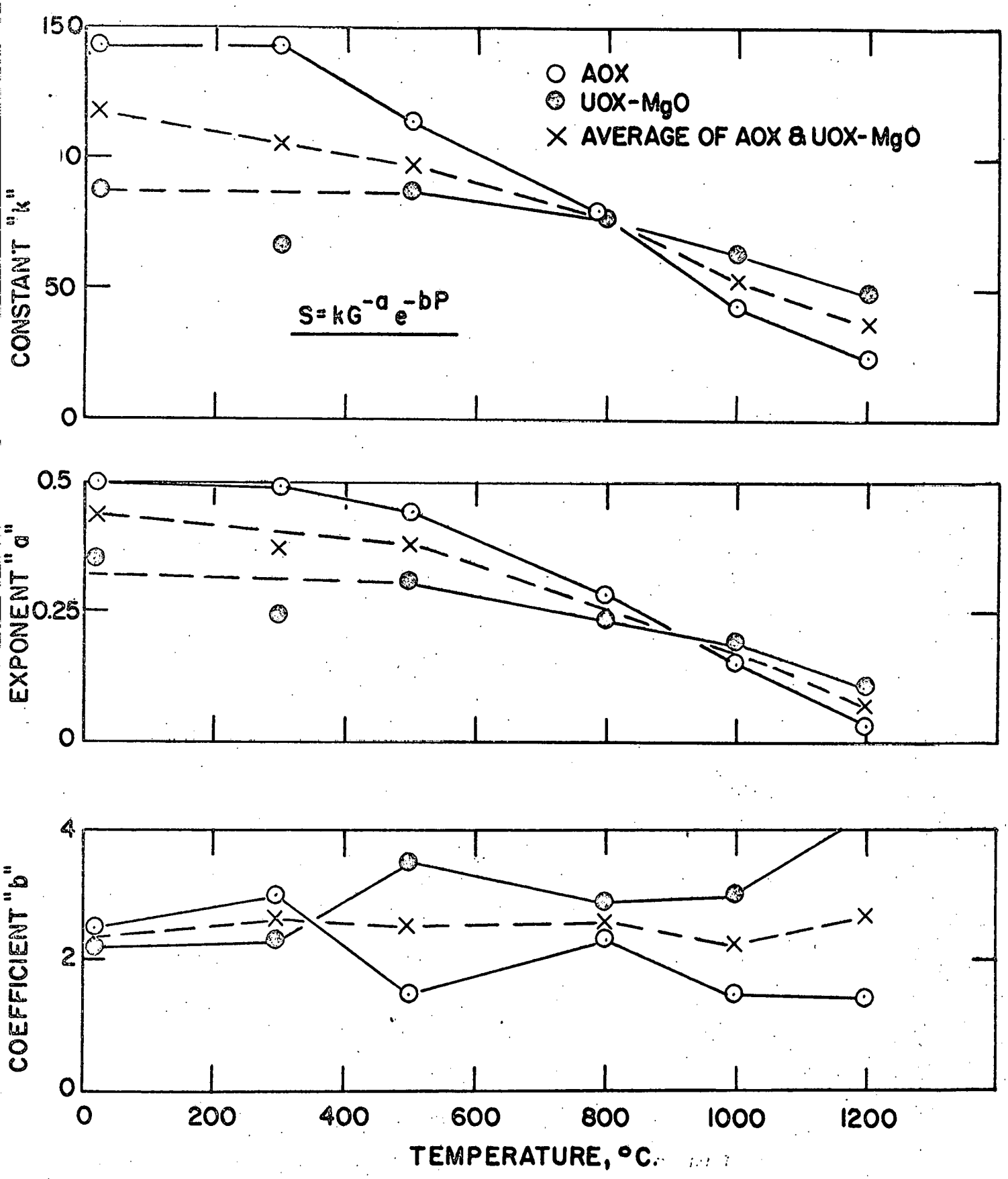
150
100
50
0
CONSTANT "k"
AOX
UOX-MgO
AVERAGE OF AOX & UOX-MgO
S=kG^-a e^-bP
0.5
0.25
0
EXPONENT "a"
4
2
0
COEFFICIENT "b"
0
200
400
600
800
1000
1200
TEMPERATURE, °C.

Fig 13

the average of both grades. It can be seen that the constants "k" and "a" follow the same pattern and decrease with temperature. The constant "k" reflects the basic strength of the material, and the constant "a" the effect of grain size on the strength. The decrease in "a" indicates a decreasing dependence on grain size as the temperature increases. Since internal stresses are a function of grain size and should reduce as temperature increases, the decrease in "a" may be the result of the decrease in internal stresses.

The porosity coefficient, "b", apparently remains fairly constant, although there is considerable scatter, with increasing temperature, the average value being about -2.5. It will be noted that the constant "a" for AOX is significantly higher than that for UOX-MgO at temperatures below 800°C, indicating a greater dependency upon grain size for AOX than for UOX-MgO.

V. COMPRESSIVE CREEP

(1) Method of Measurement

Compressive creep tests were run in a conventional creep stand with one inch diameter high density alumina push rods. Specimens were the standard 0.238 inch diameter, one inch long, and were column loaded with dead weight. Ends of the specimens were square and parallel, generally within 0.0002 inch. In addition to dimensions, weight, and density, they were inspected before test and found free of flaws by X-ray and Zyglo techniques. After test, Zyglo inspection occasionally indicated some small cracks, particularly on the ends, but otherwise the specimens were intact in every respect.

The objective of these tests was primarily to study the effect of grain size, porosity, and composition variables. Consequently, all tests were performed at a single temperature, 1200°C, for a period of 500 hours. After assembly, the test rig was brought up to temperature with minimal load, then the desired load applied. At the end of the test, the rig was cooled to room temperature before removing the load. At all times, the furnace was swept out with slowly moving dried air to prevent water vapor corrosion of the BeO. That this was successful is borne out by the observation that the average weight loss was only one milligram for the typical 2.0 gram sample.

Many of the early tests were run without benefit of a satisfactory continuous record of deformation versus time. For these tests, the only reliable measurement was total deformation. Later in the program, this situation was corrected by installation of a sapphire rod dilatometer arrangement in which the moving member was in direct contact with the end of the specimen via a hole through the pushrod. Exterior to the furnace, movement was detected by a linear voltage differential transformer and the signal fed into a chart recorder.

(2) Experimental Results

Data from thirteen tests operated with the dilatometer arrangement are summarized in Table X. Seven are illustrated in Figure 14. It is apparent that the curves are fairly linear and that total deformation in most cases may be used as a good estimate of strain rate. The comparison in Table X includes strain rates (percent in 500 hours) calculated from the

TABLE X

COMPRESSIVE CREEP OF BeO SPECIMENS AT 1200°C

Material	Porosity, %	Grain Size, microns	Stress, psi	Creep, % in 500 hours (a)	(b)	(c)
AOX	14.3	6	2000	4.88	4.99	4.80
	13.1	11	3000	1.37	1.38	1.36
	7.1	3	1000	6.59	6.50	4.30
	8.3	12	3000	1.24	1.32	1.16
	5.0	8	3000	1.54	1.64	1.31
	8.3	15	6000	3.09	2.89	2.86
	14.2	15	3000	1.77	1.72	1.73
UOX-MgO	15.0	9	3000	0.92	0.91	0.85
	15.0	7	3000	2.56	2.54	2.10
	3.8	11	3000	0.33	0.46	0.33
	7.9	5	2000	1.52	1.54	0.67
	7.4	11	6000	1.31	1.30	1.22
	2.2 (d)	20	6000	0.36	0.38	0.25

(a) Total change in length of sample.

(b) Total deflection on chart recorder.

(c) Calculated from constant strain rate portion of curve.

(d) Isostatic pressed and sintered.

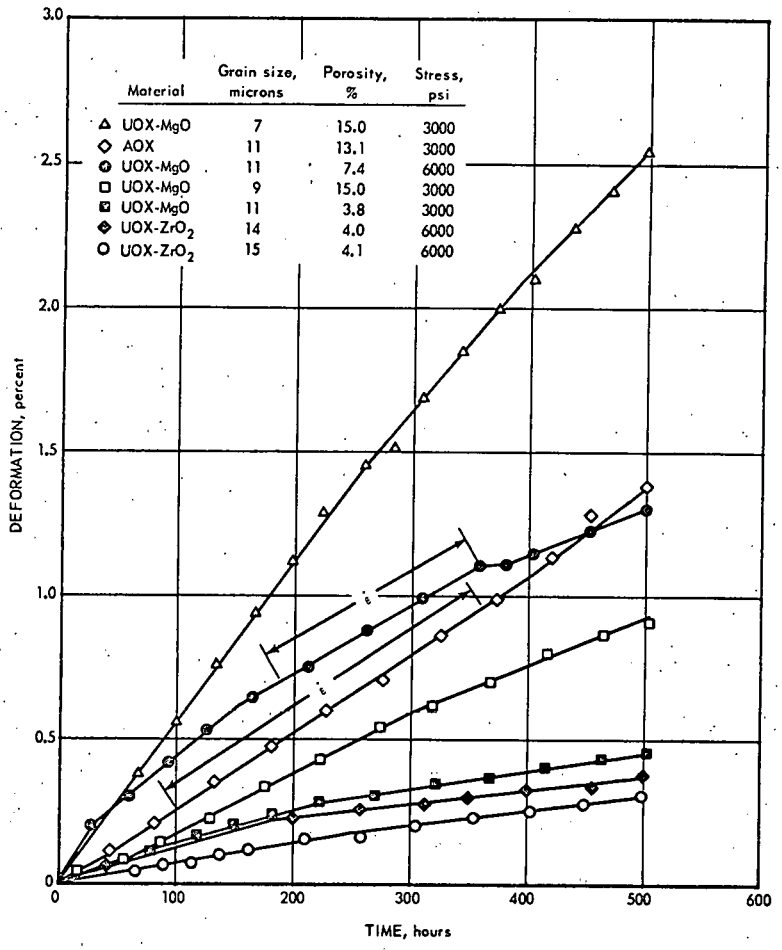
Material
Grain size, microns
Porosity, %
Stress, psi
UOX-MgO 7 15.0 3000
AOX 11 13.1 3000
UOX-MgO 11 7.4 6000
UOX-MgO 9 15.0 3000
UOX-MgO 11 3.8 3000
UOX-ZrO2 14 4.0 6000
UOX-ZrO2 15 4.1 6000
DEFORMATION, percent
TIME, hours
0
0.5
1.0
1.5
2.0
2.5
3.0
100
200
300
400
500
600

Fig 14

limiting slopes of the time curves, with two exceptions as noted in Figure 14. On the basis of this comparison, and recognizing the scatter of data which otherwise exists, all test runs are reported, including those for which total deformation is the only available measurement. These tests are summarized in Table XI. Included are results for four tests of specimens of UOX containing 3 weight percent ZrO_2.

(3) Discussion of Results

If one equates total deformation with strain rate, it is possible to discuss the data in terms of the Nabarro-Herring relationship[25] which states that strain rate, $\dot{\epsilon}$, is proportional to stress, σ , and the diffusion coefficient of the diffusing species, D, and inversely proportional to the square of the grain size, μ. This is valid if creep is diffusion controlled, and is expressed as follows:

$$\dot{\epsilon} = \frac{K D\sigma}{\mu^2 kT} \qquad (12)$$

where K is a proportionality constant which includes the volume of the diffusing species. At a single temperature, both T and D are constant, and it is apparent that strain rate should be a linear function of the parameter $\frac{\sigma}{\mu^2}$.

The experimental data may be manipulated in various ways. For example, strain rates (total deformation in 500 hours) may be normalized to a single grain size according to the above expression. Such normalized data plotted versus stress should be a straight line. In actual fact, such a plot (not

TABLE XI

COMPRESSIVE CREEP OF BeO SPECIMENS AT 1200°C

Grain Size, microns	Density, g/cm³	Porosity, %	Stress, psi	Parameter, psi/microns²	Creep,[a] percent in 500 hr
AOX					
3	2.80	7.1	1000	111.0	6.59[b]
6	2.58	14.3	2000	55.6	4.88[b]
8	2.86	5.0	3000	46.9	1.54[b]
10	2.87	4.7	6000	60.0	2.47[b,c]
11	2.62	13.1	3000	24.8	1.37[b]
12	2.76	8.3	3000	20.8	1.24[b]
15	2.87	4.8	3000	13.3	0.62
15	2.76	8.3	6000	26.7	3.09[b]
15	2.56	14.2	3000	13.3	1.77[b]
16	2.88	4.4	1000	3.9	0.18
17	2.79	7.3	3000	10.4	0.30
18	2.76	8.4	3000	9.3	0.37
18	2.78	7.6	6000	18.5	0.46
18[d]	2.75	8.6	8000	24.7	0.71
20	2.93	2.8	6000	15.0	0.36
33	2.90	3.6	3000	2.8	0.07
35	2.67	11.3	8000	6.5	1.34
39	2.65	12.1	10000	6.6	1.20
41	2.97	1.4	3000	1.8	0.03
42	2.91	3.5	6000	3.4	0.09
46	2.97	1.4	2000	0.95	0.03
71	2.94	2.3	10000	2.0	0.11
79	2.92	3.0	10000	1.6	0.12
UOX-MgO					
5	2.77	7.9	2000	80.0	1.52[b]
7	2.56	15.0	3000	61.2	2.56[b,c]
9	2.56	15.0	3000	37.0	0.92[b,c]
11	2.90	3.8	3000	24.8	0.33[b,c]
11	2.79	7.4	6000	49.6	1.31[b,c]
13	2.94	2.5	6000	35.5	0.25
15	2.60	13.6	6000	26.7	0.47
17	2.90	3.8	3000	10.4	0.23
19	2.90	3.6	8000	22.2	0.69
20[d]	2.94	2.2	6000	15.0	0.36[b]
38	2.72	9.7	10000	6.9	0.17
38	2.86	5.1	10000	6.9	0.26
47	2.92	3.1	10000	4.5	0.07
63	2.77	8.0	10000	2.5	0.05
89	2.94	2.2	10000	1.26	0.07

TABLE XI (Cont.)

COMPRESSIVE CREEP OF BeO SPECIMENS AT 1200°C

Grain Size, microns	Density, g/cm^3	Porosity, %	Stress, psi	Parameter, psi/microns^2	Creep,[a] percent in 500 hr
UOX-ZrO_2					
14	2.93	4.0	6000	30.6	0.19[c]
15	2.93	4.1	6000	26.7	0.22[c]
19	2.94	3.3	3000	8.3	0.07
21	2.95	3.1	6000	13.6	0.09

(a) Column loading on specimens one inch long by 0.238 inch diameter. Tested in dry air.

(b) Further details given in Table X.

(c) Deformation versus time shown in Figure 14.

(d) Isostatic pressed and sintered.

shown) suggests that at stresses greater than 6000 psi, strain rate depends on stress raised to a power greater than unity. This is particularly apparent in the AOX data. Also, two tests attempted at 15000 psi resulted in specimen failure during the first twenty hours. Taken together, these observations suggest that above a stress level of 6000 psi, microcracking may occur which leads to enhanced deformation rates and in the extreme case, catastrophic failure.

Secondly, there is a strong suggestion in the data that samples of very small grain size (< 10 microns) exhibit total deformations more than expected on the basis of results obtained with coarser structures. Evidence is implicit in Table X in which the greater disagreements between total deformation (a) observed and (b) calculated from constant strain rate curves occur for the smallest grain size samples in each group. In part, this disagreement is accounted for by the fact that the small grain size samples undergo some additional sintering at 1200°C. The magnitude of this shrinkage was separately determined in thermal soak tests but was found insufficient in most cases to account for the anomalous behavior. This "anomaly" is therefore considered real, and is similar to that discussed above with respect to Young's modulus and modulus of rupture, all three perhaps a manifestation of a different type of porosity distribution.

Third, there is the possibility that specimens with a high degree of porosity will deform more rapidly than specimens with low porosity. In Figure 15, all data are presented, and tests in the above categories are considered anomalous and coded separately according to the arbitrary descriptions:

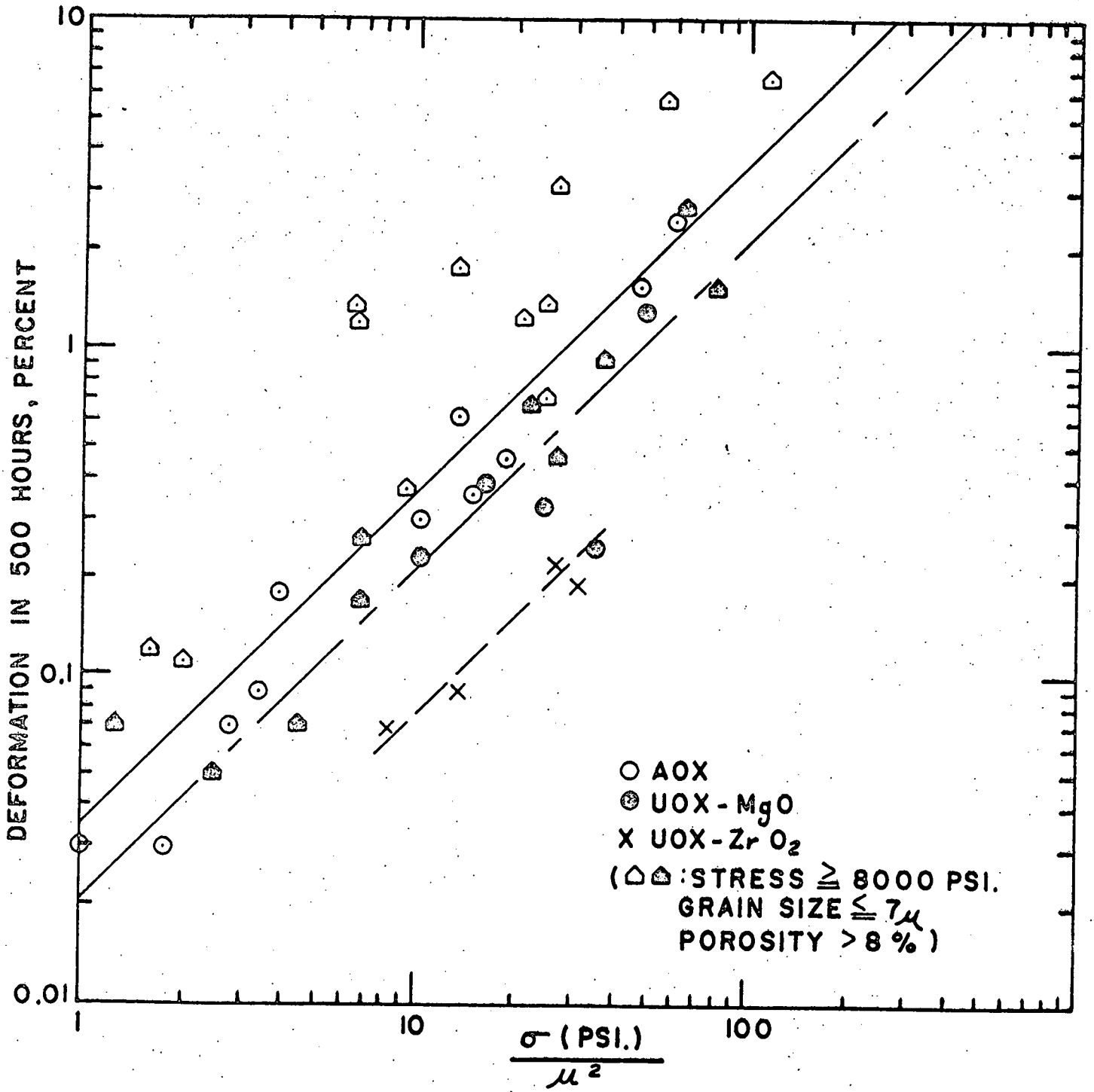
10
1
0.1
0.01
DEFORMATION IN 500 HOURS, PERCENT
1
10
100
σ (PSI.) / μ²
○ AOX
◉ UOX - MgO
X UOX - Zr O₂
(△▲ : STRESS ≧ 8000 PSI.
GRAIN SIZE ≦ 7μ
POROSITY > 8 %)

Fig 15

(a) stress $\geq$ 8000 psi

(b) specimen $\leq$ 7 micron grain size

(c) specimen > 8% porosity

Figure 15 is a log-log plot of total deformation in 500 hours versus the parameter psi/μ^2. If the anomalous points are ignored, lines with unit slope, as drawn, are good representations of the data for the three types of specimen*. This is considered evidence that compressive creep at 1200°C is a diffusion controlled process according to the Nabarro-Herring relationship.

It is interesting to note that the anomalies are more pronounced for AOX than for UOX-MgO although in both groups of specimens similar ranges in grain size, porosity, and stress were included.

Since the data satisfy the requirements of the Nabarro-Herring relationship, it is pertinent to review the data for UOX-MgO with respect to the phenomenon of preferred grain orientation. If the degree of orientation were affecting strain rate, samples of small and large grain size would not fit a plot such as Figure 15 with unit slope since degree of orientation varies with grain size. Putting it another way, data for UOX-MgO should separate into a family of such unit slope curves, each corresponding to a different grain size. However, inspection of the data indicates that there is no trend with grain size.

*For AOX, the data points could perhaps be better represented by a straight line with a slope greater then unity, but this would involve an unwarranted degree of confidence in those tests for which the total deformation was less than 0.001 inch.

If preferred grain orientation is not a factor in determining creep rates, the differences between the three groups of points in Figure 15 probably must be ascribed to composition differences. Using the Nabarro-Herring relationship, the following diffusion coefficients may be estimated from the lines drawn in Figure 15:

AOX	4.2×10^{-14} cm^2/sec	} at 1200°C
UOX-MgO	2.4×10^{-14} cm^2/sec	
UOX-ZrO_2	0.86×10^{-14} cm^2/sec	

These values are shown in Figure 16 together with other data from the literature, all of which were obtained at higher temperatures. The data of Chang[26] were deduced from bending creep measurements and required extrapolation from 1650°C which was his lowest temperature of measurement. The data of Austerman[27] were obtained directly from measurement of beryllium-7 penetration at temperatures ranging from 1566 to 2010°C. The particular data shown in Figure 16 were obtained for 99.3% dense BeO and are considerably lower than he found for 92.4% dense BeO. The latter are omitted from this comparison since it is felt that at the extremely high temperatures of his measurements, mechanisms other than bulk diffusion are more likely to complicate the experiments for the more porous material. The results by Vandervoort and Barmore[28] are of particular interest since the temperature range of 1370 to 1540°C is close to that of the present work. In their report, only strain rates were given; however, adequate sample descriptions were available and diffusion coefficients were estimated from the Nabarro-Herring equation. Data for eight runs designated by these investigators[28] as "standard creep tests" are shown in Figure 16. The line representative of these data is

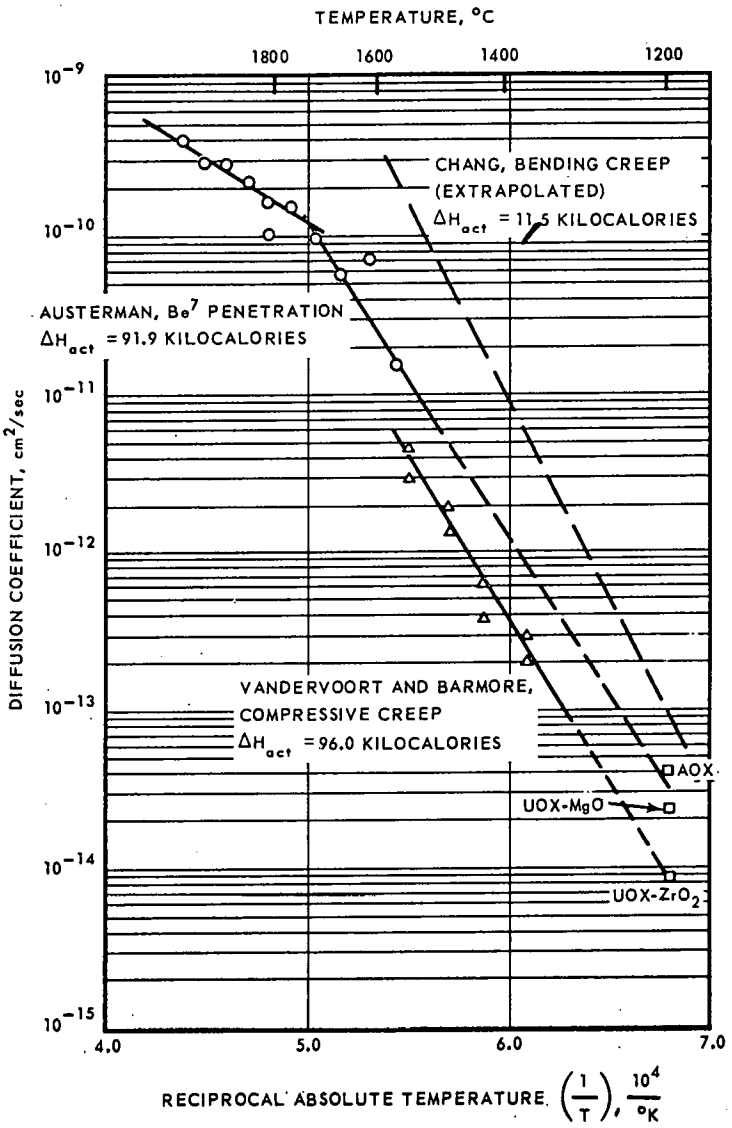
TEMPERATURE, °C
1800
1600
1400
1200
10^{-9}
10^{-10}
10^{-11}
10^{-12}
10^{-13}
10^{-14}
10^{-15}
DIFFUSION COEFFICIENT, cm^2/sec
CHANG, BENDING CREEP
(EXTRAPOLATED)
ΔH_{act} = 11.5 KILOCALORIES
AUSTERMAN, Be^7 PENETRATION
ΔH_{act} = 91.9 KILOCALORIES
VANDERVOORT AND BARMORE,
COMPRESSIVE CREEP
ΔH_{act} = 96.0 KILOCALORIES
AOX
UOX-MgO
UOX-ZrO_2
4.0
5.0
6.0
7.0
RECIPROCAL ABSOLUTE TEMPERATURE $\left(\frac{1}{T}\right), \frac{10^4}{°K}$

Fig 16

drawn with a slope corresponding to the heat of activation of 96.0 kcal/mole. The values for diffusion coefficients obtained in the present work are seen to bracket the range covered by the extrapolated lines from Austerman and from Vandervoort and Barmore. This is considered evidence that the diffusing species which determines the strain rate at 1200°C is beryllium.

VI. SUMMARY

The degree of preferred grain orientation in polycrystalline sintered BeO influences elastic constants and linear thermal expansion. Measurements of these properties, combined with pole figure determinations of grain orientation, have permitted the development of mathematical expressions relating the direction of measurement in a single crystal with Young's modulus and with thermal expansion. Young's modulus in the basal plane (a-axis) is 15% lower than in the direction of the c-axis. Thermal expansion is 13% higher in the direction of the a-axis.

These properties, as well as modulus of rupture and compressive creep, have been found sensitive to microstructural parameters of grain size and porosity. A number of empirical equations are presented to relate these various factors.

Generally, the observations are in reasonable agreement with expectations. The primary anomaly appears with the behavior of specimens of very small grain size. These exhibit lower strength than predicted by the Knudsen equations, higher creep rates than predicted by the Nabarro-Herring equation,

and somewhat lower elastic constants than larger grain size randomly oriented samples of the same porosity. This is postulated to be the result of a higher proportion of inter-granular porosity in the fine grained structures.

Acknowledgments

This work was performed under United States Atomic Energy Commission Contract No. AT(40-1)-2847.

REFERENCES

1. L.H. Sjodahl and S.F. Bartram, "Grain Orientation in Extruded BeO", J. Am. Ceram. Soc., in press.

2. B.A. Chandler, E.C. Duderstadt, and J.F. White, "Fabrication and Properties of Extruded BeO", J. Nucl. Materials, in press.

3. A.S. Creamer, "Percent Expansion of Single Crystal Alumina From 50° to 1700°C", National Bureau of Standards, unpublished (1944).

4. J.B. Wachtman, T.G. Scuderi, and G.W. Cleek, "Linear Thermal Expansion of Aluminum Oxide and Thorium Oxide From 100° to 1100°K", J. Am. Ceram. Soc., 45 [7], 319-23 (1962).

5. G.A. Chase, General Electric Company, Nuclear Materials and Propulsion Operation, Private Communication, August 1962.

6. R.F. Geller and P.J. Yavorsky, "Effects of Some Oxide Additions on the Thermal Length Changes of Zirconia", J. Res. Nat. Bur. Standards, 35, 87-110 (1945).

7. C.F. Grain and W.J. Campbell, "Thermal Expansion and Phase Inversion of Six Refractory Oxides", Bureau of Mines RI-5982 (1962), 21 pages.

8. H. Braekken and O. Jore, "Röntgenuntersuchungen über thermische Ausdehnung von Zinkoxyd und Berylliumoxyd", Det Kongelige Norske Videnskabers Selskab Skrifter, Part I, Paper #8, 8 pages (1935).

9. S.C. Carniglia and J.E. Hove, "Fabrication and Properties of Dense Beryllium Oxide", J. Nucl. Materials, 4 [2], 165-176 (1961).

10. J. Elston and R. Caillot, "Physical and Mechanical Properties of Sintered Beryllia Under Irradiation", International Conference on the Peaceful Uses of Atomic Energy, 2nd Geneva, Proceedings Vol. 5, 345-66 (1958).

11. W. Boas, "Physics of Metals and Alloys", pages 94-96, John Wiley & Sons, Inc., New York, 1947, 193 pages.

12. K.T. Miller, "High Temperature X-ray Diffraction Investigation of BeO", NAA-SR-MEMO 5934, December 1960, 3 pages.

13. S. Spinner and W.E. Tefft, "A Method for Determining Mechanical Resonance Frequencies and for Calculating Elastic Moduli from These Frequencies", Proceedings of the American Society for Testing and Materials, 61, 1221-1238 (1961).

14. R.M. Spriggs, "Effect of Open and Closed Pores on Elastic Moduli of Polycrystalline Alumina", J. Am. Ceram. Soc. 45, [9], 454, (1962).

15. D.P.H. Hasselman, "Discussion on the Porosity Dependence of the Elastic Moduli of Polycrystalline Refractory Materials", J. Am. Ceram. Soc., 45, [9], 452-454, (1962).

16. J. Lillie, "Some Properties of Beryllium Oxide", Lawrence Radiation Laboratory, UCRL-6457 (Unclassified), 14-16, May 19, 1961.

17. R.F.S. Hearmon, "The Elastic Constants of Anisotropic Materials II", Advances in Physics, 5, 323-382, (1956).

18. L.H. Sjodahl and B.A. Chandler, "Single Crystal Elastic Constants of BeO from Polycrystalline Measurements", Submitted for publication J. of Am. Ceram. Soc., March 1963.

19. D.A. Berlincourt, "Research on Piezoelectricity Materials and Phenomena", Sandia Corp. Final Report, SC-4443 (RR), p. 22 (1960).

20. D.I. Bolef, N.T. Melamed, and M. Menes, Westinghouse Research Laboratories, "Elastic Constants of Hexagonal Cadmium Sulfide", Bull. Am. Phys. Soc., 5, 169, (1960).

21. S.B. Austerman, D.A. Berlincourt, and H.H. Krueger, "Polar Properties of BeO Single Crystals", J. Appl. Phys., 34, p. 339, (1963).

22. G.G. Bentle, "Some Elastic Properties of BeO at Room Temperature", J. of Nuc. Materials, 6, [3], 336-337, (1962).

23. R.L. Coble, "Effect of Microstructure on the Mechanical Properties of Ceramic Materials", Ceramic Fabrication Processes, W.D. Kingery, ed., Massachusetts Institute of Technology, p. 222, (1958).

24. F.P. Knudsen, "Dependence of Mechanical Strength of Brittle Polycrystalline Specimens on Porosity and Grain Size", J. of Am. Ceram. Soc., 42, 376-387, (1959).

25. C. Herring, "Diffusional Viscosity of a Polycrystalline Solid", J. Appl. Physics, 21, 437-45 (1950).

26. R. Chang, "High Temperature Creep and Anelastic Phenomena in Polycrystalline Refractory Oxides", J. Nucl. Materials, 1 [2], 174-81 (1959).

27. S.B. Austerman, "Diffusion of Beryllium in Beryllium Oxide", NAA-SR-5893, May 1961, 38 pages.

28. R.P. Vandervoort and W.L. Barmore, "Compressive Creep of Polycrystalline BeO", UCRL-6748, March 1962, 24 pages.

FIGURE CAPTIONS

Fig. 1. Mean thermal expansion coefficient for BeO.

Fig. 2. Mean thermal expansion coefficient from 25 to 1200°C versus grain size for AOX and UOX-MgO.

Fig. 3. Demonstration of linear correspondence between axial expansion and percent c-axis orientation.

Fig. 4. Anisotropy of BeO thermal expansion coeffient.

Fig. 5. Anisotropy of BeO thermal expansion.

Fig. 6. AOX data fit to (1) a linear equation, (2) Spriggs' exponential equation, and (3) Hasselman's equation relating Young's modulus to porosity and compared to an earlier literature survey made by Lillie.

Fig. 7. Young's modulus for polycrystalline BeO as a function of percent orientation of the c-axes with the axis of extrusion.

Fig. 8. Comparison of Young's and shear modulus as a function of temperature with Atomics International and Argonne National Laboratory data reported by Lillie.

Fig. 9. Calculated Young's modulus for single crystal BeO as a function of the angle of measurement from the c-axis. Measured values (normalized to BeO curve) for CdS single crystals are presented for comparison of shape.

Fig. 10. Ratio of modulus of rupture at temperature to modulus of rupture at 20°C as a function of temperature for UOX-MgO and AOX segregated by "small", "medium", and "large" grain size.

Fig. 11. Modulus of rupture as a function of temperature for UOX-MgO and AOX segregated by "small", "medium", and "large" grain size.

Fig. 12. Mean values and the maximum spread in the modulus of rupture of UOX-MgO at 20°C at the 5 nominal grain sizes at 3.7% porosity are compared to the least square fit of the Knudsen equation. Limits at 95% confidence are shown for the line and for the scatter of points about the line. The two other nominal porosity curves are shown for comparison.

Fig. 13. Behavior of the constant "k", grain size exponent "a", and porosity coefficient "b" in the Knudsen strength equation, $S = k\, G^{-a} e^{-bP}$, as a function of temperature for modulus of rupture of UOX-MgO and AOX.

Fig. 14. Compressive creep deformation vs. time at 1200°C.

Fig. 15. Percent creep in 500 hours at 1200°C as function of stress and grain size; $\left(\frac{\text{psi}}{\text{microns}^2}\right)$.

Fig. 16. Comparison of data for bulk diffusion coefficient in BeO.